Investigating gravitational grabens related to lateral spreading and evaporite dissolution subsidence by means of detailed mapping, trenching, and electrical resistivity tomography (Spanish Pyrenees)

F. Gutiérrez[1], R. Linares[2], C. Roqué[3], M. Zarroca[2], J. Rosell[4], J.P. Galve[5], and D. Carbonel[1]
[1]DEPARTAMENTO DE CIENCIAS DE LA TIERRA, UNIVERSIDAD DE ZARAGOZA, EDIFICIO GEOLÓGICAS, CALLE PEDRO CERBUNA 12, E-50009 ZARAGOZA, SPAIN
[2]DEPARTAMENTO DE GEOLOGÍA, UNIVERSIDAD AUTÓNOMA DE BARCELONA, E-08193 BARCELONA, SPAIN
[3]ÀREA DE GEODINÀMICA EXTERNA I GEOMORFOLOGIA, UNIVERSITAT DE GIRONA, CAMPUS MONTILIVI, E-17071 GIRONA, SPAIN
[4]CALLE DE LA PENYA 3, E-25691, ÀGER, LLEIDA, SPAIN
[5]DIPARTIMENTO DI SCIENZE DELLA TERRA, UNIVERSITÀ DEGLI STUDI DI MODENA E REGGIO EMILIA, MODENA 41100, ITALY

ABSTRACT

The active lateral spread of the Peracalç Range (Spanish Pyrenees) has developed on a Cretaceous limestone sequence around 250 m thick, underlain by tectonically thickened (~2.5 km) Triassic halite-bearing evaporites and clays. Outward expansion of the Triassic sequence by ductile deformation and probably halokinesis toward the debuttressed and unloaded front of the range has been accommodated in the overlying cap rock through the development of a striking horst and graben morphostructure. Fault scarps show anomalously high height to length ratios (aspect ratio; H_{max}/L) compared to the values reported for tectonic faults. This retrogressive gravitational deformation has aborted a paleodrainage, expressed as wind gaps, hanging valleys, and defeated streams. The significant vertical displacement component in this rock spread is attributed to subsidence caused by interstratal evaporite dissolution, as supported by the dissolution-induced collapse and graben structures mapped at the foot of the range. To our knowledge, the rock spread of Peracalç, covering around 4.5 km^2 and with a minimum volume of 0.9 km^3, is the largest documented landslide of the Pyrenees. The excavation of trenches and the acquisition of electrical resistivity tomography profiles provided information on the thickness and subsurface structure of the graben fills, the age of the lateral spread (older than 45 ka), an unexpected episodic kinematic behavior of the gravitational faults, and the timing of deformation events, including slumping of lake deposits.

LITHOSPHERE; v. 4; no. 4; p. 331–353. | Published online 4 June 2012. doi: 10.1130/L202.1

INTRODUCTION

Rock spreads (Varnes, 1978; Pasuto and Soldati, 1996) or block spreads (Cruden and Varnes, 1996) typically develop on slopes consisting of brittle rocks underlain by soft formations (Fig. 1). The laterally unconfined soft rock, under the load of the overlying rigid slab, may expand outward, eventually producing a bulge. This extension is accommodated in the overlying cap rock through the retrogressive development of tensile fractures subperpendicular to the displacement direction and the dragging apart of the intervening blocks. The separation of the rigid slab into blocks may occur through preexisting tectonic fractures or newly formed gravitational joints (e.g., Conti and Tosatti, 1996). As spreading progresses, a horst and graben morphostructure controlled by synthetic and antithetic gravitational faults may develop (McGill and Stromquist, 1979; Moore and Schultz, 1999; Micallef et al., 2007). The lateral extension of the soft rock unit is accompanied by vertical contraction, leading to subsidence of the overlying rigid rocks (Schultz-Ela, 2001). Frequently, expansion and vertical flattening attenuate away from the free face, and consequently subsidence increases toward the free face of the slope, leading to downward flexure of the rock slab and/or outward toppling of the decomposed blocks (Fig. 1). The cracks between the blocks may be filled by soft material squeezed up from below or detritus falling from above. Lateral spreads are clearly complex landslides, since they are affected by different types of displacement (translation, subsidence, and rotation), and frequently evolve into other movement types (i.e., topples, rock falls, rotational slides, and earth flows; Rohn et al., 2004). However, they are sufficiently distinctive and endemic to certain geological situations to be considered as a separate landslide typology (Varnes, 1978; Cruden and Varnes, 1996).

Extension of the plastic unit may be related to continuous visco-plastic deformation of argillaceous sediments (Radbruch-Hall, 1978; Varnes, 1978; Záruba and Mencl, 1982), deformation across multiple discontinuity planes and shear zones (Alves and Lourenço, 2010), and the development of closely spaced dilation joints (Mège et al., 2011). More diverse deformation mechanisms may be involved when the brittle cap rock is underlain by soluble evaporitic formations. In these contexts, low-yield-strength salt-bearing evaporites may flow due to differential loading (Harrison, 1927; Huntoon, 1982; Hudec and Jackson, 2007). Moreover, the rigid blocks may undergo substantial subsidence due to interstratal evaporite dissolution favored by enhanced water percolation in the fissured and faulted slope affected by lateral spreading (Fig. 1).

In this paper, we analyze for the first time the Peracalç Range lateral spread, which is to our knowledge the largest slope movement in the Spanish Pyrenees. The Peracalç landslide is a peculiar gravitational slope deformation with excellent examples of gravitational grabens related to both lateral spreading and

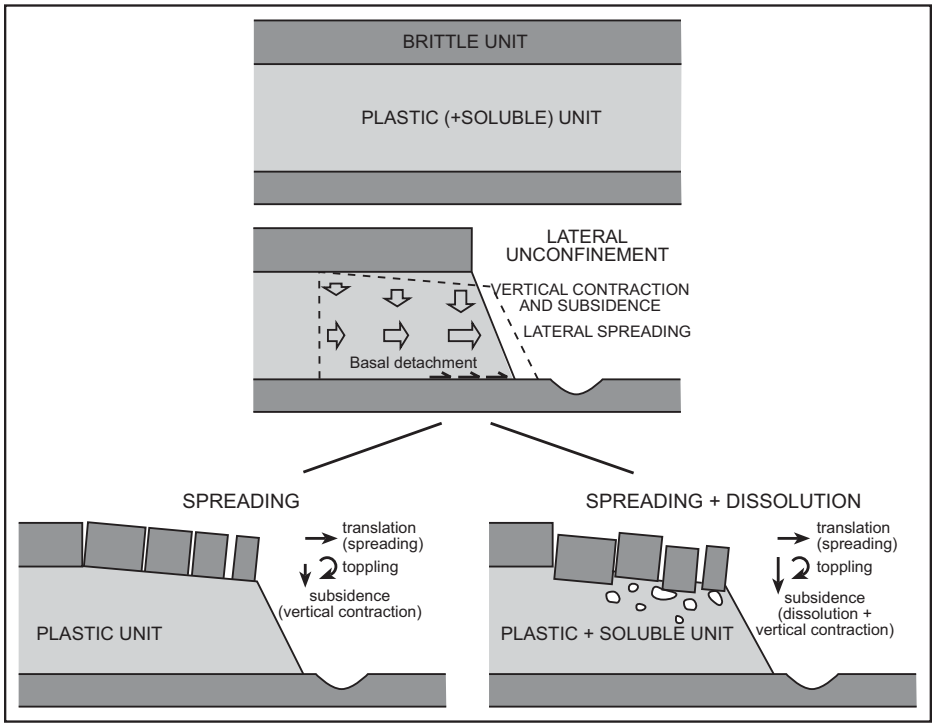

Figure 1. Evolutionary sketch showing the main displacement components in a lateral spread related to the outward expansion of a plastic unit as well as a plastic and soluble formation affected by interstratal karstification. Lateral extension is accompanied by vertical contraction, with the consequent translation, subsidence, and outward rotation of the spreading blocks. The subsidence of cap-rock blocks may reach significantly higher magnitudes if the underlying evaporitic unit is affected by interstratal dissolution.

subsidence due to interstratal dissolution of halite-bearing evaporites. The paper also documents grabens and collapse structures at the foot of the range related to interstratal evaporite dissolution. These gravitational structures, despite their extent (>5 km^2) and geological significance, have been overlooked in previous geological maps and studies. According to our literature review, this is the first rock spread investigated by means of trenching and electrical resistivity tomography (ERT). The main objectives of the work include: (1) characterizing the grabens developed in the lateral spread of Peracalç Range and the evaporite dissolution collapse structures formed at the foot of the range; (2) analyzing the processes and factors involved in the gravitational deformation phenomena, as well as their impact on drainage network development; (3) obtaining information on graben-fill thickness, deformation style, kinematic behavior (progressive versus episodic), and timing of deformation by means of trenching and ERT; and (4) exploring criteria that might be useful to differentiate between gravitational (nonseismogenic) and tectonic (seismogenic) faults. This work illustrates that rock spreads underlain by evaporites may generate significant normal faults with episodic displacement showing structural and geomorphological characteristics similar to those of tectonic origin. However, a good understanding of the geological context and some anomalously high parameters (e.g., height/length ratio of fault scarps, horizontal separation, long-term horizontal and vertical displacement rates) may help to diagnose their gravitational origin, ruling out the seismogenic potential.

REVIEW ON ROCK SPREADS

Rock spreads generally develop on stratigraphic sequences that have a nearly horizontal structure or a slight downslope dip. Mauduit et al. (1997), analyzing a large submarine lateral spread in the Gulf of Guinea and based on analogue physical models, concluded that the basal slope angle (i.e., dip of the base of the salt unit) controls both the width of the area affected by lateral spreading and the faulting pattern ("raft tectonics"). For slope angles above a threshold value, wide lateral spreads with three distinctive domains develop—an upslope graben system with synthetic and antithetic listric normal faults, a central raft, and a downslope sequence of half grabens controlled by synthetic listric faults.

Several case studies reveal that large rock spreads may form in low-gradient slopes (Cancelli and Pellegrini, 1987). For instance, Pánek et al. (2008) reported on a lateral rock spread with an estimated volume of 400×10^6 m^3 in the Crimean Mountains, Ukraine, in a slope with an average gradient of 6° including the headscarp. The development of rock spreads may be favored by a number of factors, such as: (1) lateral unconfinement or debuttressing of the soft rock unit due to erosion or uplift by active faulting (Delgado et al., 2011; Carobene and Cevasco, 2011); (2) increased precipitation and water percolation through fissures, with the consequent softening of the argillaceous rocks (Pasuto and Soldati, 1996) (a similar effect is expected with the presence of evaporites, which may also dissolve, reducing the mechanical strength [Tran et al., 2011] and causing subsidence of the overlying rocks); (3) weakening of argillaceous rocks due to expansion and contraction of smectite clay minerals (Pánek et al., 2008); (4) fluvial incision, resulting in a lowering of the water table in evaporitic formations and an increase in the hydraulic gradient, inducing higher groundwater flow rates and favoring karstification (Gutiérrez et al., 2012); and (5) seismic shaking (Micallef et al., 2007; Cauchon-Voyer et al., 2011).

Pasuto and Soldati (1996), in their review on rock spreads, indicated that displacement rates for these types of slope movements are typically between 0.1 mm/yr and 10 cm/yr. According to Cruden and Varnes (1996), block spreads are characterized by extremely low displacement rates (<16 mm/yr). In the rock spread of the grabens of Canyonlands, Utah, Marsic et al. (2003), combining global positioning system (GPS) and differential interferometric synthetic aperture radar (DInSAR), measured a maximum horizontal deformation rate of 6 mm/yr and a relative regional subsidence of up to 3 mm/yr, in agreement with the data presented by Furuya et al. (2007). Rohn et al. (2004), for a lateral spread developed on calcareous rocks underlain by marls and halite-bearing clays (northern Calcareous Alps, Austria), recorded mean horizontal displacement rates of 11.4 mm/yr using GPS. Delgado et al. (2011), applying DInSAR, measured average displacement rates between 0 and 2 mm/yr in a lateral spread in southern Spain, and recognized a slight acceleration after a rainfall episode equivalent to the average annual precipitation. Viero et al. (2010) indicated that the displacement rate in the active Cinque Torri lateral spread, Italian Dolomites, is too slow to be measured by means of GPS over a monitoring period of 3 yr. Vlcko (2004), in

the lateral spread that constitutes the foundation of the United Nations Educational, Scientific, and Cultural Organization (UNESCO) site Spis Castle, Slovakia, reported average dilation rates from 0.27 to 3.25 mm/yr for specific fissures using crack gauges. Petro et al. (2004) recorded mean horizontal separation rates of 0.19 mm/yr in fissures equipped with crack gauges for a lateral spread developed in the Strechovy volcano, Slovakia. Displacement in lateral spreads is partitioned in multiple fissures, and consequently measurements from cracks constitute partial and minimum values of the overall gravitational deformation. In spite of the low velocity, continuous displacement on spreading slopes may constitute a threat to any engineering structure, including dams, tunnels, pipelines, or transportation infrastructure. The zones of maximum differential displacement can be preliminarily recognized with a reasonable level of confidence by means of detailed geomorphological mapping. Lateral spreads can also have significant hydrological implications, since they may disrupt surface drainage, create internally drained depressions, and enhance focused water infiltration along extensional fractures.

To our knowledge, the largest documented subaerial rock spread is the grabens of Canyonlands, Utah, with an estimated volume of 60 km^3 (Cruden and Varnes, 1996) and a minimum age of 65 ka (Biggar and Adams, 1987). This lateral spread has developed at the eastern margin of the 360–530-m-deep Cataract Canyon of the Colorado River. Here, the exposed stratigraphic sequence has a gentle dip (~2°–4°) toward the canyon and consists of a 460-m-thick brittle sandstone sequence lying on the salt-rich evaporite Paradox Formation. Extension in the upper rigid plate caused by lateral flow of the salt formation toward the unloaded canyon has generated an arcuate system of grabens covering around 200 km^2 (McGill and Stromquist, 1979; Moore and Schultz, 1999; Baars, 2000). The flow of the Paradox Formation due to differential loading has produced the Meander anticline, the sinuous axis of which coincides with the channel of the Colorado River (Harrison, 1927; Huntoon, 1982). Differential subsidence due to interstratal evaporite dissolution in this area, largely dominated by subsurface drainage, must play a relevant role in the development of the grabens and the downward flexure of the sandstone plate, as indicated by the presence of saline springs in the bottom of Cataract Canyon and the large throw documented on some faults (≥145 m; Grosfils et al., 2003). The grabens, up to 6 km long and 500 m wide, are bounded by en echelon fault arrays. The progressive growth of en echelon fault segments eventually led to their overlapping and linkage through the rupture of relay ramps in the stepover zones (Fossen et al., 2010). Moreover, the deeply dissected tributary canyons of the Colorado River expose fissures filled with cemented detrital deposits up to 250 m deep (Ely, 1987). Wind gaps at the top of the horsts provide evidence for a deformed and abandoned paleodrainage, which has been used, together with knick points, to analyze the impact of the gravitational deformation on the drainage network evolution (Trudgill and Cartwright, 1994; Cartwright and Mansfield, 1998; Trudgill, 2002), and to reconstruct the kinematic behavior of fault arrays (Commins et al., 2005).

Even larger lateral spreads related to the downslope flow of salt formations underlying brittle rocks have been documented in continental shelves of passive margins. In the Gulf of Guinea, an Upper Cretaceous–Tertiary sedimentary cover has spread laterally above an Aptian salt unit along a stretch more than 200 km long across the continental margin front. Here, spreading is accommodated through the development of grabens for which a long-lasting deformation history is recorded by the overlying synkinematic sedimentary sequence (Mauduit et al., 1997). In the Gulf of Mexico, the sedimentary units overlying a halokinetic Jurassic salt formation (Louann Salt) have spread basinward since Mesozoic times, resulting in the development of an ~1000-km-long arcuate system of grabens with the convexity pointing landward. These gravitational grabens, controlled by normal faults rooted in the salt detachment, have been mapped both offshore and onshore (Diegel et al., 1995; Rowan et al., 1999).

Mège et al. (2011) documented lateral spreads at the edge of Jabi and Kebenawa mesas in Ethiopia, where a limestone and sandstone cap rock, 400–450 m thick, is underlain by a laterally unconfined gypsiferous formation that is around 300 m in thickness. Features indicative of lateral spreading and dissolution-induced subsidence in these gravitational movements include: (1) dense network of dilation joints perpendicular to the spreading direction in the gypsum unit, filled with fibrous gypsum with the axes of the crystals oriented in the direction of extension; (2) open fractures, horsts, and grabens parallel to the edge of the elongated mesas; (3) a 50–100-m-thick stratiform limestone breccia resting on the gypsiferous formation; and (4) blocks of cap rock foundered within the underlying gypsum.

GEOLOGICAL SETTING

The structure of the central Spanish Pyrenees consists of a suite of south-verging thrust sheets developed during Late Cretaceous–Miocene times as a result of the convergence and collision between the Iberian and European plates (Choukroune and ECORS, 1989). The following structural units are differentiated (Figs. 2A and 2B): The Axial zone, constituting the core of the orogen, consists of an antiformal stack of folded thrust sheets made up of Variscan basement rocks (Muñoz, 1992). Les Nogueres structural unit, situated on the southern flank of the Axial Pyrenees, forms a narrow fringe underlain by Variscan basement rocks and a Pennsylvanian–Triassic cover affected by steeply dipping and overturned thrusts and folds (Seguret, 1972). To the south, there is an extensive thrust system called the South Pyrenean unit, in which Mesozoic and Tertiary formations have been transported tectonically toward the Ebro foreland basin. The South Pyrenean unit is composed of three main thrust sheets, progressively thinner toward the south: Bóixols–Sant Corneli, Montsec, and Marginal Ranges. The study area is located astride the Les Nogueres and the South Pyrenean structural units and between the N-S–trending and deeply entrenched Flamicell and Noguera Pallaresa Rivers (Fig. 2C). In this sector, situated close to the crustal-scale Étude Continentale et Océanique par Reflexion et Réfraction Sismiques (ECORS) Pyrenees profile (Figs. 2A and 2B), the northern boundary of the South Pyrenean unit is defined by the Morreres back thrust (Muñoz, 1992; Figs. 2C and 2D). The hanging wall of the Morreres back thrust constitutes the prominent Peracalç Range, mostly composed of resistant Cretaceous limestones and Paleogene conglomerates. Conversely, the footwall of the Morreres back thrust is expressed in the landscape as an erosional strike depression excavated in more labile bedrock, dominated by Triassic argillaceous and evaporitic sediments (Figs. 2D and 3).

The lithological units exposed in the footwall of the Morreres back thrust (Les Nogueres structural unit) include (Fig. 3): (1) Silurian black slates, which crop out in the NE sector of the mapped area; (2) Upper Permian and Lower Triassic red detrital rocks of the Buntsandstein facies; (3) the Middle Triassic Muschelkalk facies, which is 50–100 m thick and consists of well-stratified gray micritic and bioturbated limestones with intercalated dolomites (units 2 and 3 are combined in Fig. 3 as nonevaporitic Triassic); and (4) the Upper Triassic Keuper facies, composed of argillaceous and evaporitic sediments (Calvet et al., 2004; Salvany and Bastida, 2004). The nearby Erinyà-1 oil exploration borehole (Fig. 2C) and the tectonic models proposed by Saura (2004) and Beamud et al. (2011) for this sector of Les Nogueres structural unit suggest that the tectonically thickened Triassic evaporitic succession in the study area may reach 2500 m. Ductile deformation, subsurface

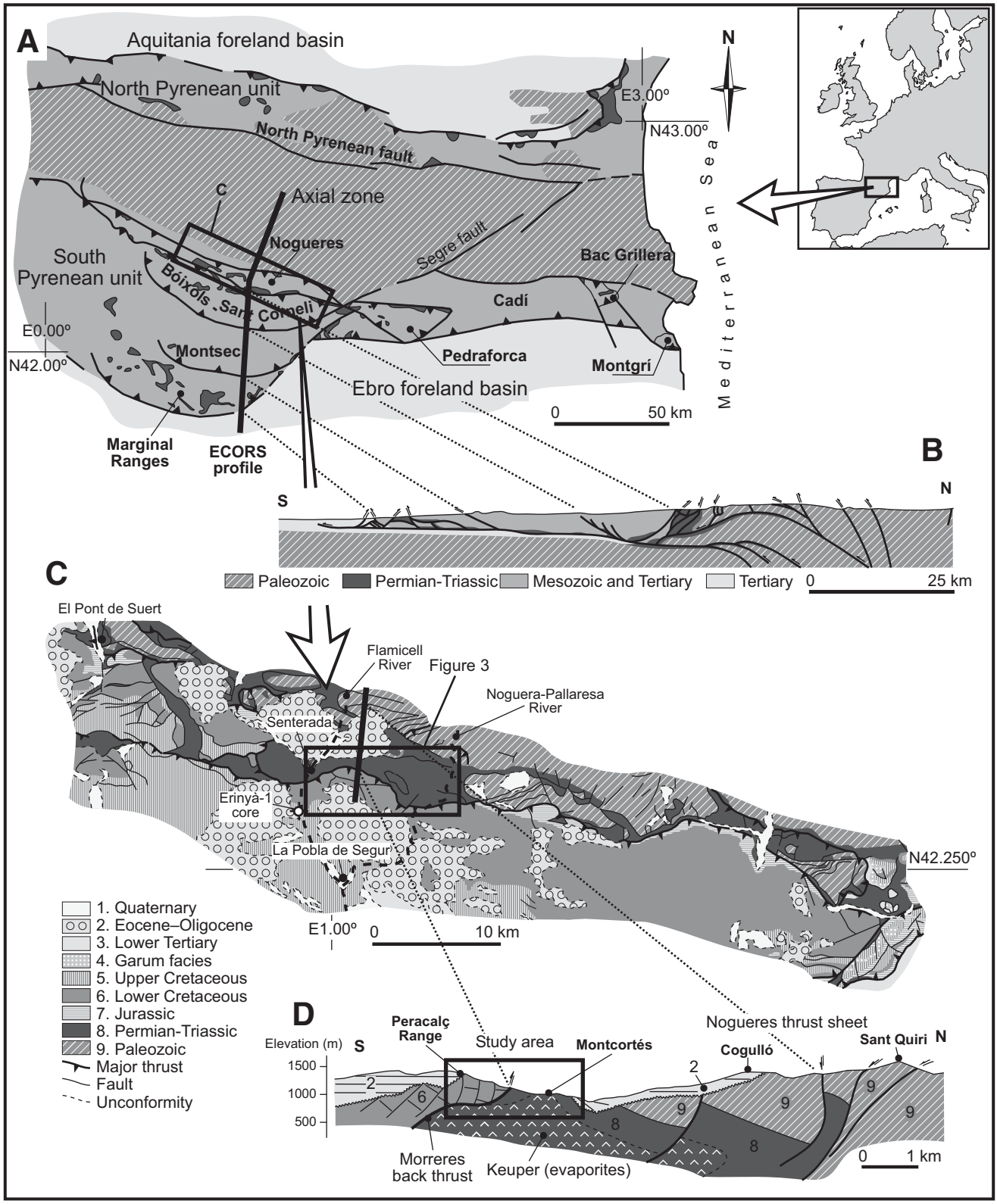

Figure 2. Geological setting of the study area. (A) Geological sketch of the Pyrenees showing the main structural units (after Rosell and Linares, 2001). The most extensive outcrops of Permian–Triassic evaporites, and the general location of the study area (bold rectangle), which is traversed by the Étude Continentale et Océanique par Reflexion et Réfraction (ECORS) seismic profile, are indicated. (B) N-S geological cross section synthesizing the ECORS profile (after Berástegui et al., 1993). (C) Simplified geological map of the Les Nogueres structural unit showing the location of our study area (bold rectangle) (after Rosell, 1963, 1970, 1994; García-Senz, 2002). (D) Schematic geological cross section of the study area (after Rosell, 1994).

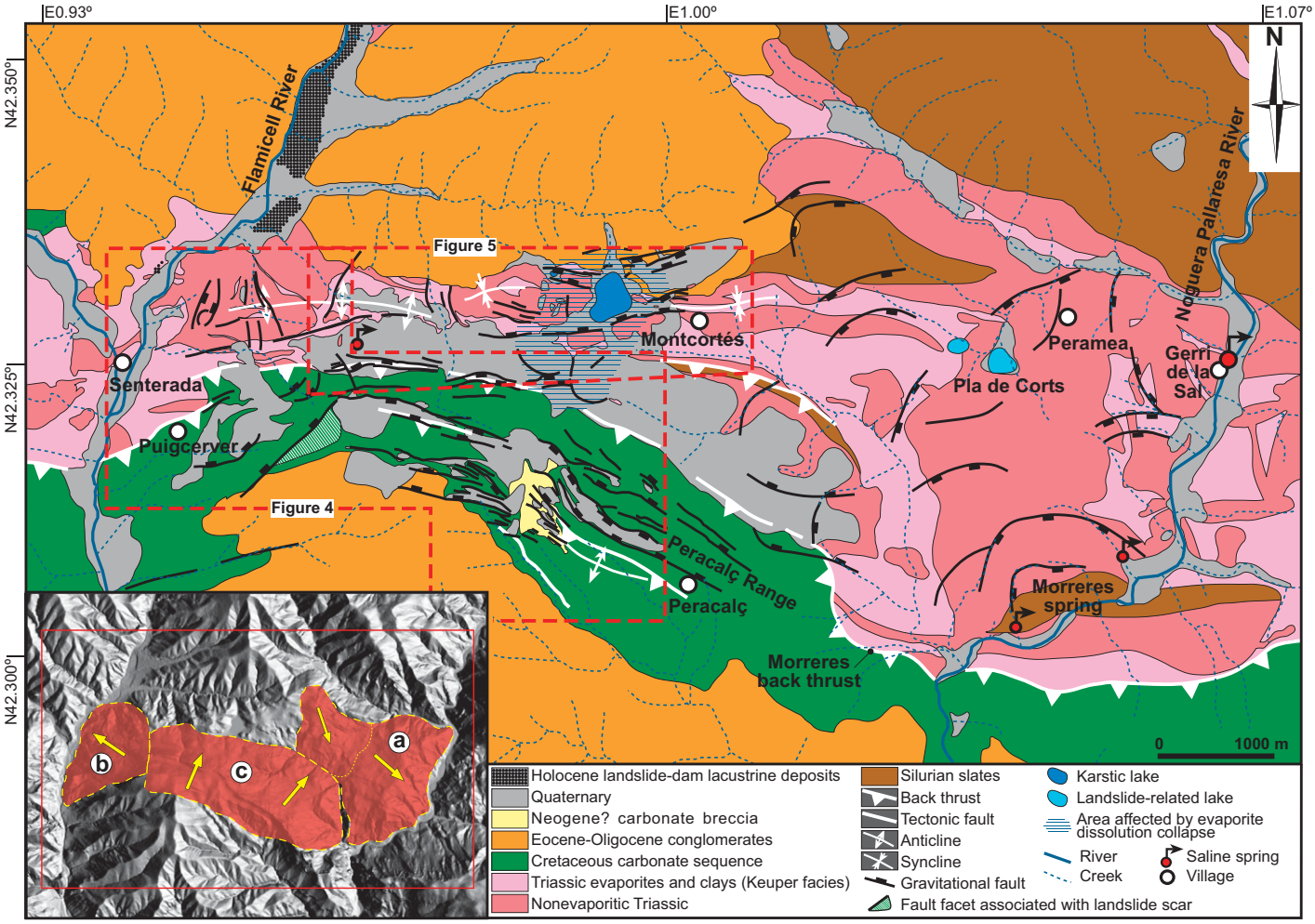

Figure 3. Geological-morphostructural map of the Senterada–Gerri de la Sal erosional depression and adjoining reliefs between the Flamicell and Noguera Pallaresa fluvial valleys. Map is elaborated from previous works (Rosell, 1970, 1994; Saura, 2004; García-Senz, 2002), with addition of new field data. Inset: Main deep-seated landslide complexes differentiated in this study in the Senterada–Gerri de la Sal erosional depression (shown as bedrock in the color map): (a) Gerri de la Sal–Peramea landslide; (b) Puigcerver-Senterada landslide; (c) Peracalç Range lateral spread.

dissolution, and probably also halokinesis of this formation have played an instrumental role in the development of the investigated gravitational deformations. In outcrop, the Keuper facies displays reddish and multicolored clays with secondary gypsum. Klimowitz and Torrescusa (1990), based on borehole data from the South Pyrenean unit, differentiated a lower evaporitic unit with a high proportion of halite and an upper clay unit with anhydrite. The highly variable thickness of the lower evaporitic unit recorded from boreholes seems to be related to local tectonic thickening and probably halokinesis: 465 m in Surpirenaica-1 borehole, 30 km west of the study area, and 1240 m in Isona-1 borehole, 25 km to the south. The upper clay unit reaches 130 and 200 m in these boreholes, respectively. Although there are no borehole data from the study area, the presence of halite at depth is proven by the saline springs of Morreres and Gerri de la Sal, in the Noguera Pallaresa valley (Fig. 3). The latter is used for the production of salt. Most likely, the exposed sediments of the Keuper facies correspond to a condensed residual sequence resulting from the vanishing of the most soluble evaporites by dissolution, as is commonly the case in many salt-bearing evaporitic formations (Warren, 2006; Gutiérrez and Cooper, 2012).

Other lithological units exposed in the footwall of the Morreres back thrust include (5) relatively small bodies of dolerites (ophites) intruded within the Keuper facies and mostly attributed to sills injected in Triassic times (Hartevelt, 1970) and (6) the Paleozoic and Mesozoic formations on both sides of the Morreres back thrust, which are unconformably overlain by Oligocene conglomerates deposited in alluvial-fan environments, i.e., the Pyrenean Molasse (Rosell and Riba, 1966; Saura and Teixell, 2000). These detrital sediments once covered most of the Paleozoic and Mesozoic rocks in the study area, before the excavation of the Senterada–Gerri de la Sal depression. The conglomerates situated north of Montcortés village correspond to the d'Envall Conglomerates, which are Oligocene in age (Rosell, 1963, 1970; Saura and Teixell, 2000; Saura, 2004; Beamud et al., 2011). This folded detrital formation, 250–550 m thick, truncates the underlying thrust faults of the Les Nogueres structural unit (Fig. 2D). It consists of scarcely cemented, massive and poorly sorted gravel with chaotic fabrics, including meter-sized boulders mostly derived from the Lower Triassic Buntsandstein facies.

The following formations have been mapped in the hanging wall of the Morreres back thrust (South Pyrenean unit) (Fig. 4A): (1) The exposed Jurassic rocks are restricted to small outcrops

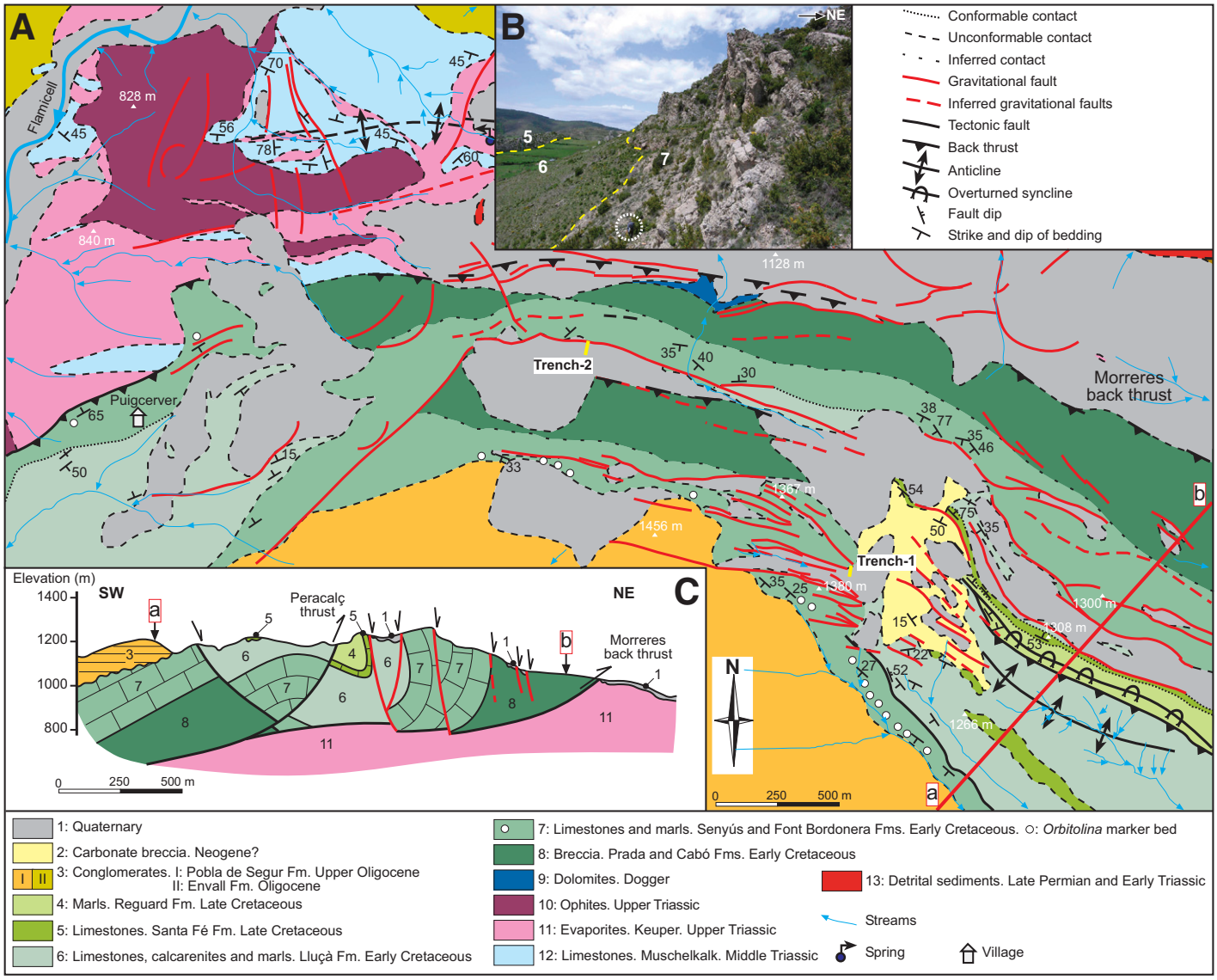

Figure 4. (A) Geological map of the Peracalç-Puigcerver area. See location in Figure 3. (B) Image of the overturned northern limb of the Peracalç syncline showing distribution of the formations Senyús–Font Bordonera (7), Lluçà (6), and Santa Fé (5). Circled person for scale. (C) Geological cross section a-b across the eastern sector of Peracalç Range, covering a broader transect than the map. Cross section based on Rosell (1963), García-Senz (2002), Saura (2004), and our new data.

of Middle Jurassic (Dogger) black dolomites associated with the Morreres back thrust. The Erinya-1 oil exploration borehole (Lanaja et al., 1987), located just next to the southwestern edge of the study area (Fig. 2C), penetrated a Jurassic sequence, 1600 m thick, with an upper anhydrite unit 700 m in thickness. This evaporitic unit might be present at depth beneath the Peracalç Range (hanging wall of the Morreres back thrust) and could have played a role in the development of the analyzed deep-seated slope movements. (2) The Early Cretaceous carbonate succession (Aptian-Albian), with a stratigraphical thickness of around 1000 m, constitutes most of the outcropping rocks in the Peracalç Range. Detailed mapping of these units and gravitational fault scarps has been instrumental for the identification and characterization of the deep-seated slope movements affecting the brittle carbonate sequence underlain by the ductile and soluble Keuper facies. The differentiation of lithostratigraphic units is based, with some simplifications, on the stratigraphic framework established in previous works (Rosell, 1963, 1970, 1994; Mey et al., 1968; Garrido and Ríos, 1972; Peybernés, 1976; Martínez, 1982; Rosell and Llompart, 1982; Bernaus et al., 2000; García-Senz, 2002). (2a) The early Aptian Prada and Cabó Formations, around 500 m thick, consist of gray and blackish micritic limestone with marls. This stratigraphic unit associated with the Morreres back thrust frequently exhibits a thick, massive, and chaotic breccia composed of large blocks embedded in red clays. Locally, blocks of Jurassic units are recognized within these breccias. Several nonexclusive interpretations can be proposed for this unit: a tectonic breccia related to shearing caused by the underlying back thrust; a dissolution and collapse breccia generated by the karstification of the underlying Triassic evaporites; or a rauhwacke resulting from the dissolution of the evaporitic components once incorporated in a tectonic breccia associated with a thrust controlled by a lubricating evaporite formation (Warren, 2006). Similar

breccias have been documented by Canérot et al. (2005) in the Lauriolle diapir, French Pyrenees. (2b) The Senyús and Font Bordonera Formations (late Aptian–Albian), 300 m in cumulative thickness, have been grouped as a single cartographic unit. The Senyús Formation (late Aptian) is made up of micritic limestones with a small proportion of intraclasts and bioclasts. In the Flamicell valley, it overlies the Keuper facies (Fig. 4A). The Font Bordonera Formation (late Aptian–Albian) consists of gray limestones and marls with a hardground at the top, which includes a significant accumulation of glauconite. (2c) The Albian Lluçà Formation, 250 m thick, is composed of alternating limestones and calcarenites with some grainstone and marl layers. The top of this unit corresponds to an erosional surface on which Late Cretaceous limestones were deposited disconformably. (2d) The Late Cretaceous sedimentation is recorded by the Cenomanian Santa Fé limestones and the Turonian Reguant marls, ~25 m and 50 m thick, respectively (Rosell, 1963, 1970, 1994; Berástegui et al., 1990; García-Senz, 2002). (3) In the upper and southern sector of the Peracalç Range, the marine Cretaceous succession is unconformably overlain by Upper Oligocene conglomerates of the Pobla de Segur Formation. This massive, poorly sorted, and polymictic conglomerate fills a paleovalley, locally reaching 3500 m in thickness (Mellere and Marzo, 1992). The lithology of the clasts, dominated by Early Cretaceous carbonates and including Paleozoic and Triassic rocks, indicates a provenance from the north.

The study area, situated in a key sector at the boundary between the South Pyrenean and Les Nogueres units, has been the subject of several detailed structural maps (García Senz, 2002; Saura, 2004). These two papers show notable discrepancies and present disparate tectonic models. In our opinion, this lack of concordance is partly due to the presence of large deep-seated gravitational slope deformations superimposed on the tectonic structures, which have been overlooked by previous authors. An additional source of discrepancy is the difficulty of differentiating the Early Cretaceous formations in the field.

Detailed geological mapping reveals that the Cretaceous formations in the eastern sector of the Peracalç Range, hanging wall of the Morreres back thrust, are affected by NW-SE–trending folds and thrusts related to the underlying Morreres back thrust (Muñoz, 1988) and superimposed on Cretaceous synsedimentary extensional faults (Berástegui et al., 1990; Saura, 2004) (Figs. 4A and 4C). Most of the gravitational normal faults and grabens in this sector of the Peracalç Range are located in its northern laterally unconfined frontal zone, where the topographic relief is greatest and the carbonate rocks are underlain at relatively shallow depth by thick Triassic evaporites and clays.

East and west of Montcortés village, the Permian–Triassic rocks in the footwall of the Morreres back thrust display an antiformal syncline, the Bellera anticline of Saura (2004) (Fig. 5). The evaporitic Keuper facies constitutes the core of the antiform, whereas the younger Muschelkalk facies crops out in the limbs and crest of the fold. The northern limb of this reversed antiform is unconformably onlapped by tilted Oligocene conglomerates. In the surroundings of Montcortés Lake, the Permian–Triassic rocks and the overlying Oligocene conglomerates are affected by gravitational grabens and ring faults with conspicuous geomorphic expression. These structures and the Montcortés Lake basin, superimposed on the previous tectonic folds, are attributed to collapse processes caused by interstratal dissolution of evaporites (Keuper facies).

METHODOLOGY

The investigation was carried out in the following phases. Initially, the main landslide complexes and subsidence morphostructures related to interstratal karstification of evaporites were recognized on the basis of previous geological maps (Rosell, 1963, 1994) and the geomorphological interpretation of aerial photographs, 1:33,000 and 1:60,000 in scale, taken in 1956 and 2002, respectively (Fig. 3). The resulting cartographic scheme was used to select the most interesting areas for the production of more detailed maps. This investigation is focused on the graben depressions generated by lateral spreading and dissolution-induced subsidence in the Peracalç Range and those resulting from collapse caused by interstratal karstification of evaporites in the Montcortés Lake area. Subsequently, 1:5000 scale geological maps were produced in these areas including information on the stratigraphy and structure of the bedrock, as well as the distribution of landforms and deposits related to gravitational surface deformation (e.g., fault scarps and graben fills). These

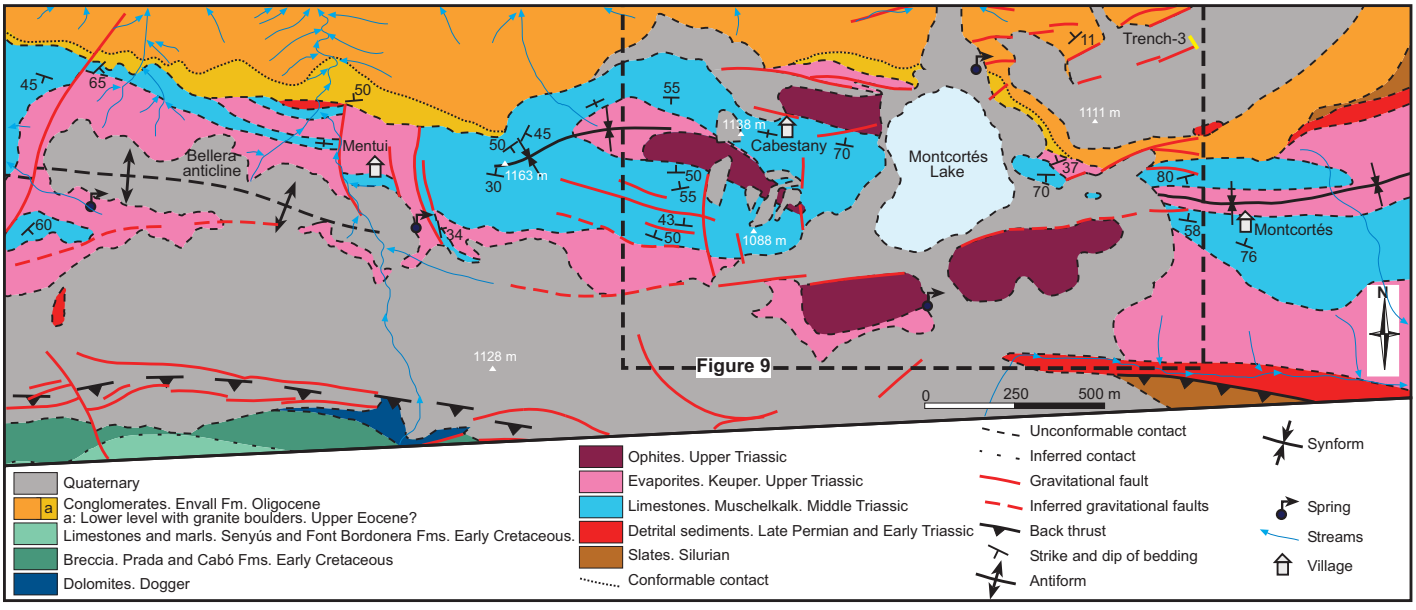

Figure 5. Geological map of the surroundings of Montcortés Lake. See location in Figure 3.

maps, covering around 13.5 km^2, have been elaborated by direct mapping in the field and partially refined using 1:18,000 and 1:22,000 aerial photographs.

In the next step, three backhoe trenches were dug across gravitational fault scarps or traversing their projected trace on recent deposits. The selection of the trench sites, two in the lateral spread of Peracalç Range (trenches 1 and 2; Fig. 6) and one at the edge of an evaporite dissolution-induced graben east of Montcortés Lake (trench 3; Fig. 5), was based on the 1:5000 geological-morphostructural maps. We followed the classical procedure applied for the study of paleoseismological trenches (McCalpin, 2009a). After cleaning the trench walls, a reference grid with horizontal and vertical strings spaced 0.5 or 1 m was placed on the shaded side of the trench, which was logged on graph paper. Material datable by the accelerator mass spectrometry (AMS) radiocarbon method or optically stimulated luminescence (OSL) was collected, preferably from the units bracketing the faulting events. The main purposes of these

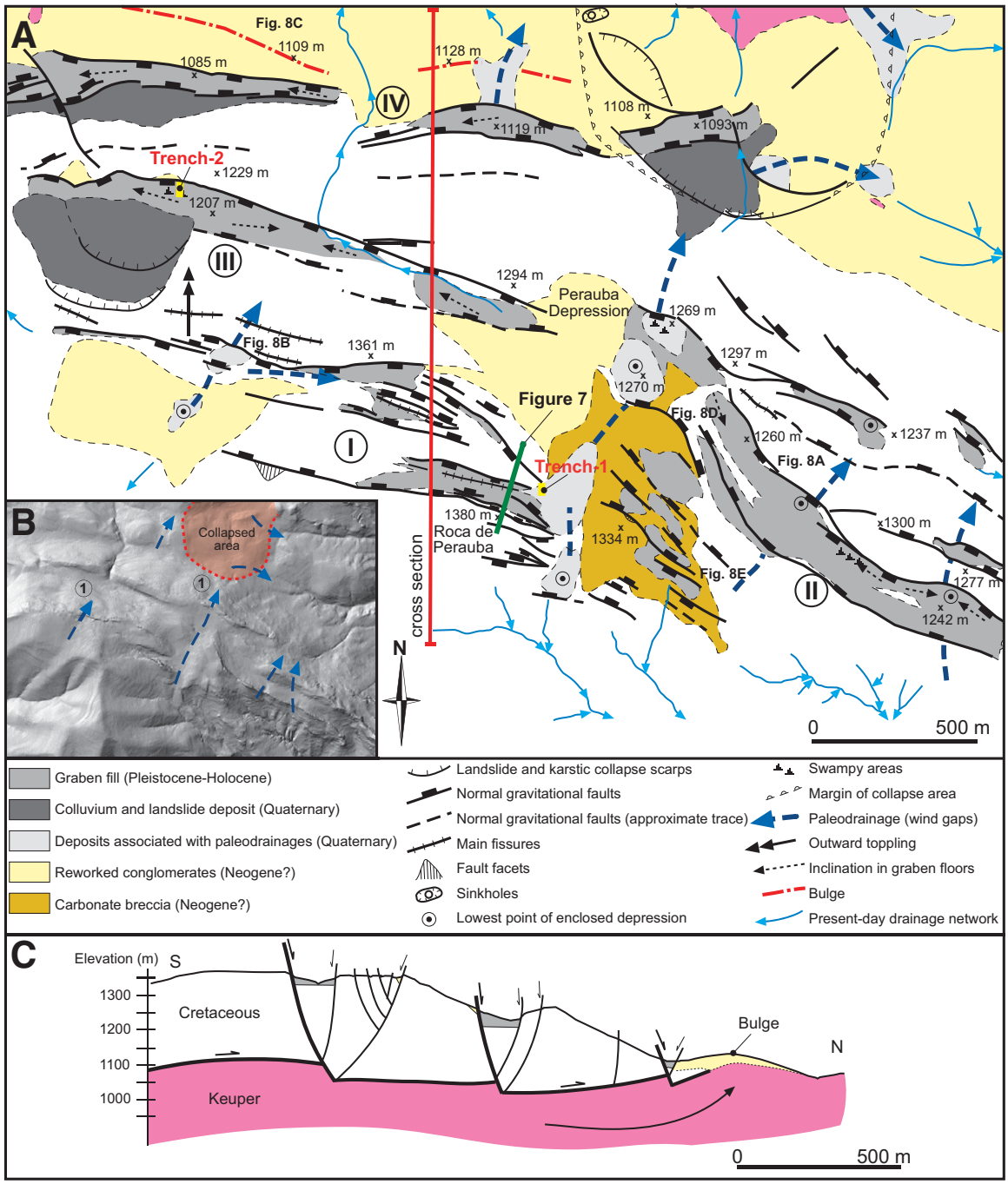

Figure 6. (A) Morphostructural map of the Peracalç Range. (B) Shaded digital elevation model indicating the main paleodrainages (arrows) disrupted by the lateral spread and the development of an evaporite dissolution collapse structure at the foot of the range. (C) Cross section of the Peracalç lateral spread.

trenches included: (1) corroborating the gravitational origin of the scarps (i.e., nonerosional); (2) analyzing the deformation style and kinematic regime (progressive vs. episodic) recorded in the trench sediments; (3) obtaining information on the chronology of the inferred deformation and sedimentary episodes through the application of numerical dating techniques; and (4) estimating slip rates. Although the trenching technique has been already applied to the study of different types of landslides, including sackung (e.g., McCalpin and Hart, 2003; Gutiérrez et al., 2008; Pánek et al., 2011; McCalpin et al., 2011), rotational slides, and translational slides (Gutiérrez et al., 2010), to our knowledge, this is the first time a lateral spreading slope movement has been investigated via trenching. In a previous paper, Gutiérrez et al. (2012) characterized a graben morphostructure generated by interstratal karstification of evaporites in the Iberian Range, Spain, by means of detailed geological-geomorphological mapping and trenching.

Finally, three electrical resistivity profiles were acquired in the two sites of the lateral spread investigated via trenching. The in-depth coverage of geoelectrical inverted models (20–50 m) has allowed us to obtain a broader insight into the subsurface structure of the investigated gravitational structures, complementing the trenching data. The two-dimensional (2-D) electrical resistivity tomography (ERT) is frequently used in the characterization of surficial deposits and shallow deformation structures (e.g., Schrott and Sass, 2008; McCalpin, 2009a; Linares et al., 2010; Van Dam, 2010; Zarroca et al., 2012). However, the application of ERT to analyze deep-seated gravitational slope deformations has rarely been undertaken (Pánek et al., 2011), and no references reporting the use of this technique in rock spreads were found in the literature review carried out for this study. The geoelectrical data were acquired with a Lund imaging system composed of a resistivity meter Terrameter SAS1000 (ABEM), and an electrode selector ES10-64e. The data acquisition was performed using a Wenner electrode array, which provides a good sensitivity for the detection of vertical heterogeneities and a good signal-to-noise ratio (Loke, 2011). The surveyed profile features are described in Table 1. The measured resistivity data set was inverted using the 2-D finite-difference inversion program RES2DINV, based on the smoothness constrained least-squares inversion implemented by using a quasi-Newton optimization technique (Loke and Barker, 1996). Technical details of the ERT method have been described in numerous earlier studies (e.g., Loke, 2011). The topographic profiles of the ERT sections were measured using a Sprinter 100 digital level of Leica Geosystems.

TABLE 1. SUMMARY OF ELECTRICAL RESISTIVITY TOMOGRAPHY (ERT) FEATURES

	Profile 1	Profile 2a	Profile 2b
Length	160 m	160 m	400 m
Array	Wenner	Wenner	Wenner
Electrode spacing*	2 m (inner reels) 4 m (outer reels)	2 m (inner reels) 4 m (outer reels)	5 m (inner reels) 10 m (outer reels)
RMS error†	1.9	1.3	4.3
Least-squares iterations	7	9	6
Total measured points	258	258	254
Depth levels	12	12	12
Approximate depth for the deepest level	24.6 m	24.6 m	61.4 m
Collection date	29 April 2008	30 April 2008	30 April 2008

*The profiles were acquired with a set of four reels: the two inner reels with 20 electrode positions each, and the two outer with 12 positions spaced double than the inner ones.
†RMS—root mean square.

GRAVITATIONAL DEFORMATION IN THE PERACALÇ RANGE AND THE SENTERADA–GERRI DE LA SAL DEPRESSION

Geological and geomorphological mapping of the Peracalç Range and the associated erosional depression between the Flamicell and Noguera Pallaresa River valleys reveals the presence of three landslide complexes covering a total area of 22 km^2 (Fig. 3, inset). The development of these anomalously large deep-seated slope movements is favored by thick (~2.5 km) halite-bearing evaporites and argillaceous sediments in the footwall of the Morreres back thrust and a high local relief generated by fluvial dissection and differential erosion; the area has not been glaciated (Bordonau, 1992; Bru et al., 1994).

The Puigcerver-Senterada landslide, covering 3.1 km^2, is located on the east margin of the Flamicell valley (Fig. 3, inset, letter c). The displaced mass includes Cretaceous and Triassic rocks of the upper and lower blocks of the Morreres back thrust, respectively. The headscarp of this landslide is defined by a prominent triangular facet, 175 m high, in the resistant limestone of the Morreres back thrust hanging wall (Fig. 3). The western margin of the Noguera Pallaresa valley is affected by the Gerri de la Sal–Peramea landslide complex (Fig. 3, inset, letter a), around 6.9 km^2 in area. This landslide mainly displaces Triassic limestones and detrital rocks, as well as the underlying clays and evaporites of the Keuper facies. The saline springs situated at the foot of the landslide strongly suggest that gravitational deformation caused by subsurface evaporite dissolution plays a significant role in the development of this slope movement.

Both the Puigcerver-Senterada and the Gerri de la Sal–Peramea landslides show large enclosed depressions with perennial lakes (i.e., Pla de Corts west of Peramea) at the foot of amphitheater-like scarps indicative of back tilting. These geomorphic features suggest that these landslide complexes correspond, at least partly, to rotational slides controlled by deep-seated failure surfaces rooted in the Triassic clays and evaporites. Assuming an ellipsoidal geometry for the sliding planes, we have tentatively estimated volumes of 0.76 km^3 and 0.27 km^3 for the Gerri de la Sal–Peramea and Puigcerver-Senterada slope movements, respectively. The convex toes of these landslides have deflected the Flamicell and Noguera-Pallaresa Rivers, showing anomalous curved traces. Lacustrine deposits mapped in the bottom of the Flamicell valley (Fig. 3), and dated at 1304–1231 cal. yr B.P. with terrestrial snail shells collected from the top of the sequence (Table 2), provide evidence for a late Holocene landslide-damming episode of the Flamicell River.

Peracalç Range Lateral Spread

In the laterally unconfined northern flank of the Peracalç Range, with a local relief of around 450 m, the carbonate sequence (250 m thick overlying plastic and soluble Triassic clays and evaporates) has spread in a NNE to NE direction toward the Montcortés depression (Fig. 4). Lateral extension has been accommodated in the brittle carbonate slab through the development of a conspicuous horst and graben morphostructure controlled by a swarm of gravitational normal faults with prevailing ENE-WSW and NW-SE trends (Figs. 4, 6, 7, and 8A). Long and fresh open fissures up to several meters wide are also common in both bedrock exposures and in the sediment-filled graben floors (Figs. 6 and 8B). The fault block topography descends in a step-wise manner toward the Montcortés depression; the bottom of the highest and lowest grabens are situated at 1332 and 1110 m above sea level (asl), respectively (Fig. 6C). In plan view, the graben system displays an overall curved arrangement with the convexity pointing downslope, similar to the trace of the Morreres

TABLE 2. CODE OF SAMPLE DATED, LOCATION, LABORATORY NUMBER (POZ—POZNAN RADIOCARBON; MAD—LABORATORIO DE DATACIÓN DE LA UNIVERSIDAD AUTÓNOMA DE MADRID), DATING METHOD, MATERIAL, CONVENTIONAL AGES, CALIBRATED RADIOCARBON DATES AT 2σ, AND CALIBRATED AGES AS YR B.P. AT 2σ (USING CALIB 6.0.1 AND THE DATA SET INTCAL 09.14C; REIMER ET AL., 2009)

Code and location	Laboratory and dating method*	Material	Conventional age (yr B.P.)	Calibrated age (yr B.P., 2σ)	OSL age (yr B.P., 2σ)
MT1-3b trench 1	Poz-22651 AMS	Charcoal	2080 ± 30	**2140–1987 (0.986)** 1976–1973 (0.004) 1958–1952 (0.01)	
MT1-2 trench 1	Poz-22650 AMS	Charcoal	70 ± 30	258–222 (0.25) **139–30 (0.73)**	
BV 1 outcrop	Poz-22471 AMS	Land snail shell	1335 ± 30	**1304–1231 (0.84)** 1208–1181 (0.15)	
MT2-3 trench 2	MAD-5406 OSL	Sands			48,674–42,328
MT2-4 trench 2	MAD-2707 OSL	Sands			17,692–15,760
MT2-5 trench 2	MAD-5806 OSL	Sands			45,518–39,376

Note: Bold type indicates calibrated age ranges with relative area higher than 0.7.
*AMS—accelerator mass spectrometry; OSL—optically stimulated luminescence.

back thrust and the tectonic structures mapped in the hanging wall (Figs. 4 and 6A). The development of this lateral spread, with a significant subsidence component, may be attributed to the following processes: (1) extension of the ductile Triassic sediments toward the laterally debuttressed front of the range, (2) halokinetic flow of the thick halite-bearing Triassic evaporitic sediments toward the unloaded foot of the Peracalç Range, and (3) differential subsidence of the fault blocks in the carbonate sequence due to interstratal karstification of the underlying evaporites. The extension would have been accompanied by vertical contraction and the consequent subsidence of the overlying carbonate sediments. The bulge mapped north of the lowermost grabens seems to be related to extension and halokinetic flow (Figs. 6 and 8C). The evaporite dissolution-induced collapse structures mapped at the foot of the Peracalç Range and in the Montcortés Lake area provide supporting evidence for this process.

The lateral spread of the Peracalç Range affects an ENE-WSW fringe around 3.8 km long, 1.1 km wide, and covering ~4.5 km^2 (Figs. 4 and 6). Its northern boundary is vaguely defined by the bulge developed at the foot of the range with a structural relief of around 50 m. The southern and eastern limits have been established on the basis of the mapped gravitational fault scarps with an orientation subparallel to that of the range. The western edge corresponds to a NE-SW–oriented and NW-facing faceted scarp related to the Puigcerver-Senterada landslide. Considering an average thickness of 200 m for the lateral spread (Fig. 6C) and excluding the uncertain thickness of Triassic sediments affected by gravitational deformation, we estimate a minimum volume of 0.9 km^3. To our knowledge, this active slope movement constitutes the largest landslide documented in the Spanish Pyrenees, exceeding the 600 hm^3 estimated for the El Ubago deep-seated gravitational slope deformation (Gutiérrez et al., 2008).

The grabens of Peracalç Range reach 1750 m in length and 400 m in width. The en echelon fault arrays bounding the graben depressions are expressed in the landscape as low-sinuosity fault scarps with very limited dissection (almost no fault facets), locally interrupted by evident relay ramps in the soft-linked stepover zones (Figs. 7D and 8D). The N-dipping synthetic faults generate downslope-facing scarps, whereas antithetic faults produce upslope-facing scarps acting as barriers for the surface runoff and sediment transport. Fault scarps reach 62 m in height (Fig. 7) and 1650 m in length. The number of faults and grabens, as well as the evidence of activity, increases toward the curved central sector of the graben system, where extension is expected to reach the highest magnitude and rate (Fig. 6A). The extensional morphostructures of the Peracalç Range closely resemble the grabens and fissures described in the grabens of Canyonlands, Utah (McGill and Stromquist, 1979; Moore and Schultz, 1999; Baars, 2000). These grabens also show an arcuate arrangement, but with the convexity pointing upslope.

Several geomorphic features indicate that the Peracalç Range used to have a N- to NE-directed drainage that has been largely disrupted by the development of transverse horsts and grabens (Figs. 6A and 6B). Evidence of the deformed and aborted paleodrainage includes: (1) perched abandoned stream courses in horst blocks (wind gaps) (Fig. 8E); (2) conspicuous knick points in drainages at the upstream margin of grabens (hanging valleys) (Fig. 8A); (3) sediment-filled closed depressions upstream of antislope fault scarps, corresponding to defeated streams (Fig. 8B), and beheaded streams recognized downstream of these fault scarps; and (4) topographically lowest areas of internally drained graben floors coinciding with paleodrainage courses, defined by wind gaps in the adjacent horsts (Fig. 6A). At the present time, the area has a very poorly developed drainage network dominated by subsurface water flow, i.e., a very low runoff coefficient. Most of the precipitation infiltrates through fissures and fractures, favoring the karstification and weakening of the underlying evaporites and clays. The course of some new streams follows graben depressions and connects with old northward-directed drainages, forming a peculiar orthogonal or trellis pattern (i.e., graben system III in Fig. 6A). Lateral spreading in the grabens of Canyonlands has caused a similar impact on the drainage network (Trudgill, 2002; Commins et al., 2005).

Using the cross section constructed across the central sector of the lateral spread (Fig. 6C), we roughly calculated the amount of extension achieved in the Peracalç Range by dip-slip displacement on the mapped normal faults. Extension related to horizontal separation on faults and fissures has been obviated due to the shortage of data. Horizontal extension (E) produced by each fault on the cross section was estimated considering a wide fault dip range ($\beta = 60°–80°$) and the vertical displacement estimated with the available topographic data (H) and assuming a nearly horizontal topography prior to faulting ($E = H/\tan \beta$). According to our calculations, the lateral spread has accommodated a cumulative horizontal extension of the order of 42–138 m, representing an increase of 3.42%–12.13% in the original length of the brittle carbonate sequence overlying the Morreres back thrust.

Four graben systems may be differentiated in the Peracalç Range (Fig. 6A). In the upper and western sector, we mapped a complex WNW-ESE–trending graben that is 1625 m long and up to 400 m wide (Figs. 6A and 6I). In total, 17 fault scarps have been mapped, together with a number of open fissures up to 280 m long. The wide open fissures developed in the northern margin of this graben indicate outward toppling of limestone blocks, with the consequent oversteepening of the slope forming its southern margin (Fig. 8B). The locally dissected scarp associated with the master synthetic fault displays one of the few triangular facets recognized in the area and developed on Oligocene conglomerates. The fault pattern shows a sharp change in the

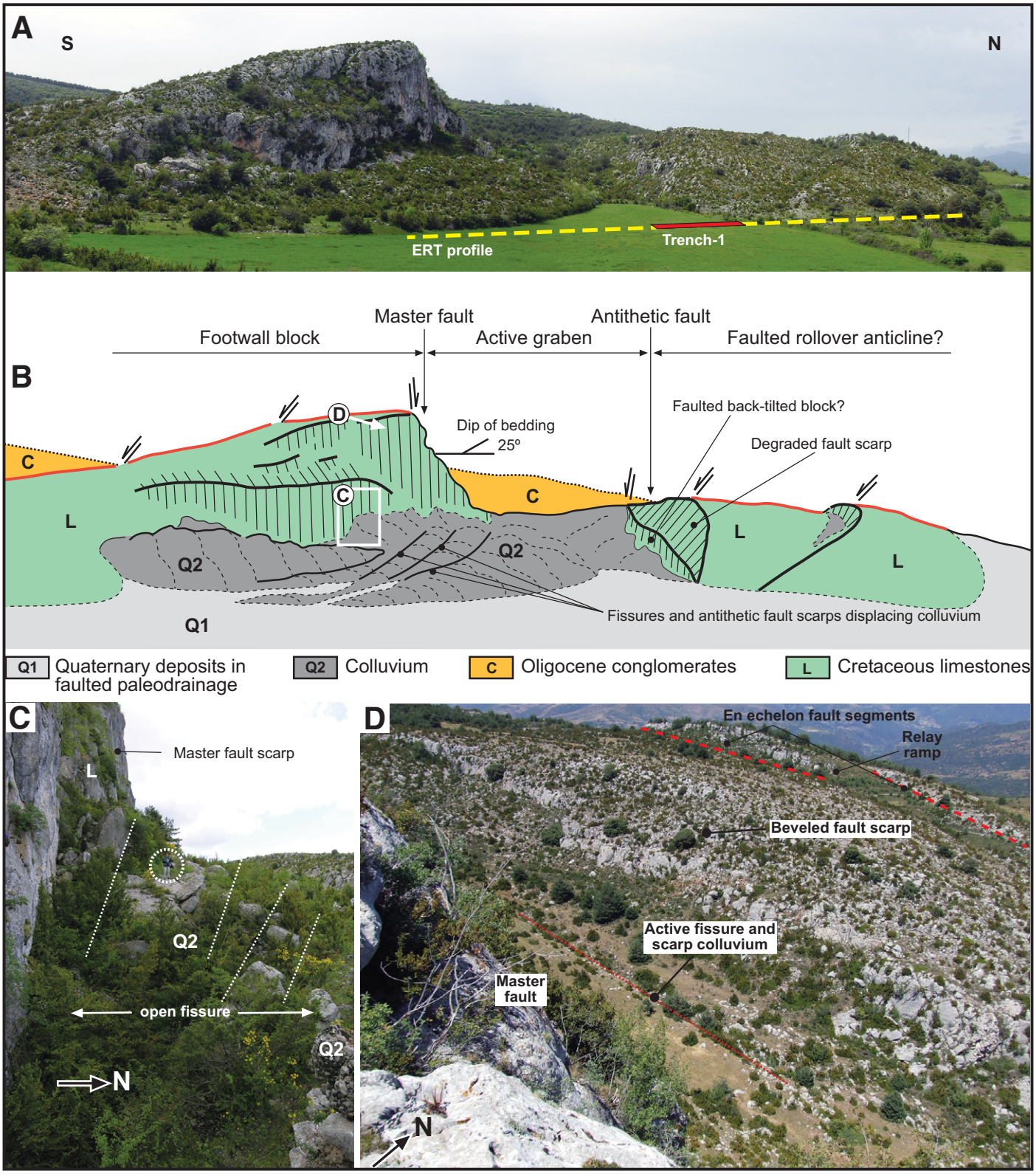

Figure 7. (A) Photograph of graben I (Fig. 6) at the head of the lateral spread showing the trace of trench 1 and profile ERT-1 (ERT—electric resistivity tomography), sited across the projection of an antithetic fault scarp in a depression related to a paleodrainage. See location in Figure 6. The colluvium at the foot of the scarp on the left (Roca de Perauba), 62 m high, is affected by multiple antislope scarps with open fissures. (B) Sketch showing the morphostructural features of the graben. (C) Open fissures in colluvium at the foot of the master synthetic fault scarp. Circled person for scale. (D) Image of the antithetic faults scarps. The antislope scarp in the central portion of the image shows a compound beveled geometry. The scarp in the foreground shows two en echelon fault segments with a relay ramp in the stepover.

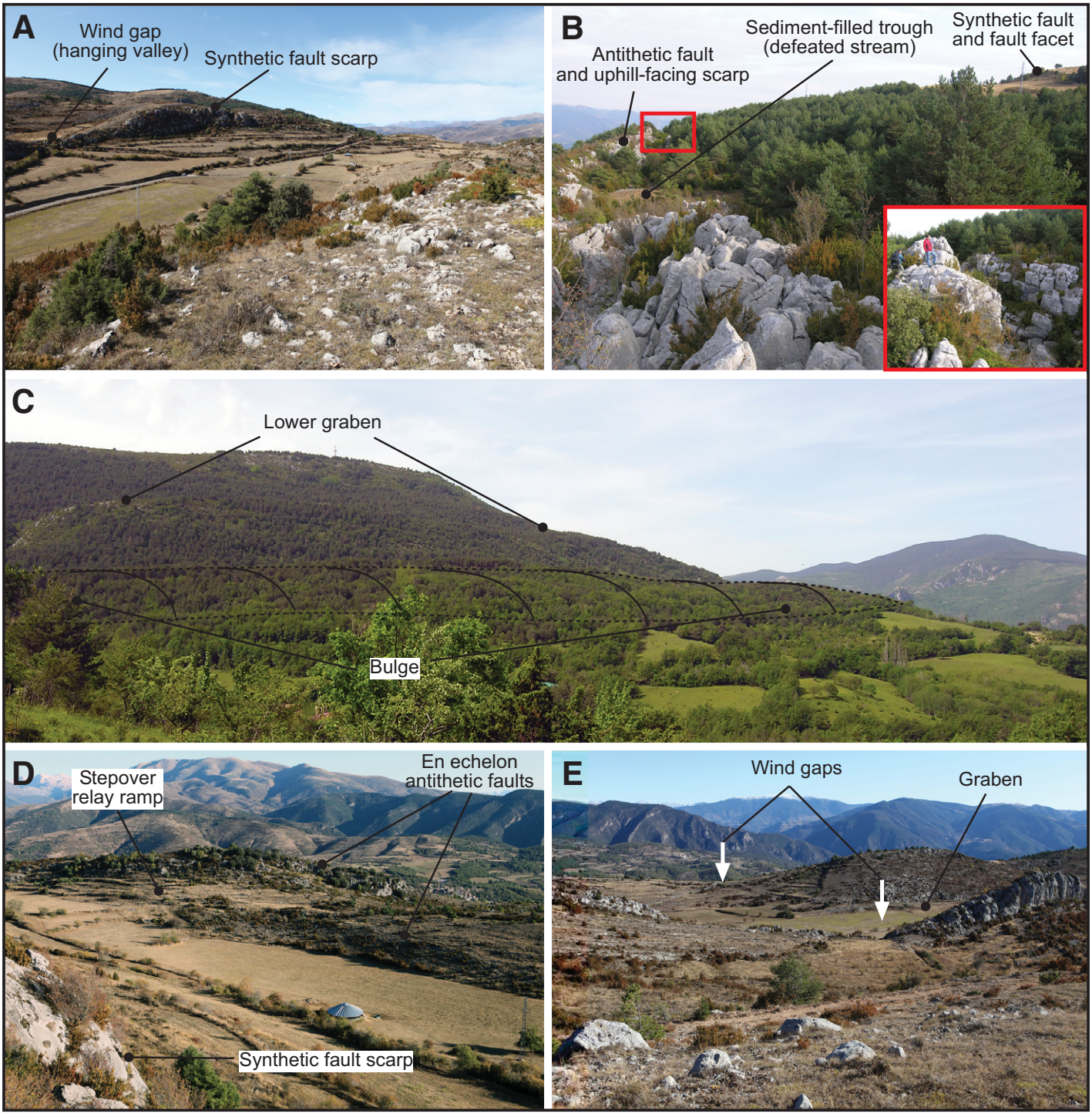

Figure 8. (A) General view of graben II (see Fig. 6A for location of all five parts of Fig. 8). Photograph taken from the upper part of the antithetic fault scarp toward the synthetic fault scarp, showing a faulted paleodrainage (hanging valley). (B) Graben I bounded by synthetic and antithetic faults. The uphill-facing scarp associated with the latter has defeated a stream generating an elongated enclosed depression. Inset shows fissure resulting from outward toppling of the block to the left. (C) Bulge at the foot of the Peracalç Range affecting a recent detrital cover. The slope above has been breached by the lower graben IV. (D) Relay ramp at the transfer zone of two en echelon fault segments (stepover) in the northern margin of graben II. (E) Wind gaps in the horsts flanking graben II.

eastern sector of this graben: (1) There are a higher number of faults, some of which adopt a NW-SE trend. (2) The graben depression is split into two grabens separated by an internal horst controlled by synthetic and antithetic secondary faults (Fig. 6C). (3) There are numerous open fissures in the graben floors. Only the largest ones have been depicted in the map. This change in the fault pattern may be partly related to spatial variations in the amount of extension and the lithology of outcropping rocks, i.e., conglomerates in the western sector and mainly limestones in the eastern zone (Fig. 4). Faulting might be partly accommodated by the development of drape folds in the conglomerates, in which fault and fold scarps degrade at a much higher rate. The eastern portion of this graben, which constitutes the head of the lateral spread, shows the most extensive and conspicuous evidence of recent deformation. The fault scarp at the southern margin of the graben reaches 62 m in height. At the foot of this nearly vertical scarp, there is a dense system of antithetic upslope-facing scarps and open fissures displacing a slightly cemented talus deposit (Fig. 7). These features seem to correspond to a keystone graben related to active vertical and horizontal displacement on the master fault. The antithetic faults in this graben locally display conspicuous beveled compound scarps and accommodation ramps in stepover or transfer zones (Fig. 7). Trench 1 was excavated on a sediment-filled depression across the eastward projection of a beveled antithetic fault scarp (Figs. 6A and 7A). An aborted paleodrainage has been inferred in the western sector of the graben through the SW-NE alignment of the following geomorphic features (Fig. 6A): the lowest point of an internally drained depression in the graben axis, an alluvium-filled enclosed depression in a defeated stream segment (Fig. 8B), and a wind gap corresponding to the beheaded stretch of the stream.

The main structure in the eastern sector corresponds to a NW-SE–trending graben that is 1750 m long and 120–205 m wide (Fig. 6A). The northeastern margin of this graben is controlled by an en echelon fault array with both soft-linked and hard-linked transfer zones. The former are expressed as relay ramps (Fig. 8D) and the latter as sharp bends in the fault scarps resulting from the linkage of fault segments through the breakage of former accommodation ramps. To the NE of this graben, there is a poorly defined horst and graben morphostructure developed on densely forested steep slopes. To the SW of the main graben we mapped a set of closely spaced and low-relief NW-SE fault scarps bounding shallow graben depressions with vague margins. In this sector, we identified a cover of locally derived carbonate detrital breccias embedded in decalcification clays of unknown age. The area deformed by the main graben used to have two SW-NE–oriented drainages, recognized by hanging valleys (Fig. 8A), the lowest points of the internally drained graben floor, and wind gaps in the horst situated to the NE (Figs. 6A and 8E). At the western edge of the graben system II, we identified a major paleodrainage revealed by the SSW-NNE alignment of sediment-filled depressions corresponding to downthrown or fault-blocked stream segments, wind gaps, and beheaded valleys (Fig. 6A).

Graben III, situated at an intermediate topographic level, may correspond to the westward projection of the main graben in sector II (Fig. 6A). This depression, controlled by left-stepping en echelon faults in the southern margin, is 1700 m long, up to 170 m wide, and has an ENE-WSW orientation. The eastern sector of the graben is drained longitudinally by a creek that exits the depression through a water gap and connects with an old S-N–oriented stream, which has been beheaded by gravitational faulting (Fig. 6A). The graben floor in its southwestern sector is overlapped by the toe of a slide. Trench 2 was excavated across the northern fault scarp of this graben.

Graben system IV includes three E-W–trending depressions situated at the lowest elevation (Fig. 6A). In this lower sector, the slopes are extensively covered by unconsolidated gravels with a fine-grained matrix derived from reworked Oligocene conglomerates. The northern margin of the central graben shows a conspicuous beheaded paleodrainage (wind gap). The eastern graben, situated at a lower elevation, has been foundered by a collapse structure defined by an arcuate scarp and related to interstratal karstification of the underlying evaporites (Figs. 6A and 6B). This subsided area forms part of the Montcortés Lake collapse area (Fig. 9). North of the western and central grabens, there is an E-W bulge (Figs. 6 and 8C). Detrital cover deposits in this sector show an open antiformal structure concordant with the topography. The occurrence of bulges is a common feature at the toe of lateral spreads (e.g., Pasuto and Soldati, 1996; Pánek et al., 2008). The development of the bulge at the foot of Peracalç Range seems to be related to the outward extrusion of the Keuper facies. This lateral and upward flow may result from both visco-plastic deformation of argillaceous sediments and halokinesis favored by differential loading (Harrison, 1927; Potter and McGill, 1978; Huntoon, 1982; Jackson, 1995; Furuya et al., 2007; Hudec and Jackson, 2007; Kirkham et al., 2002; Lucha et al., 2012).

The maximum height and length of nine uphill-facing scarps and two downhill-facing scarps were measured using a laser hypsometer (Nikon Forestry Pro) and our maps, respectively. Scarp length corresponds to the tip-to-tip straight horizontal distance. We selected the main fault scarps bounding the graben depressions and ruled out a number of downhill-facing scarps for which it was not possible to identify the location of the scarp crest due to erosional modification of the slope profile and the presence of dense forest. Aspect ratios (H_{max}/L) were plotted together with the global data set presented by Davis et al. (2005) for tectonic faults with lengths between 100 m and 10 km. The average aspect ratio of the nine uphill-facing scarps is 0.029, ranging from 0.010 to 0.063, and with a standard deviation of 0.015 (Fig. 10). Antislope scarps show a general direct relationship, with higher heights for increasing length, but with significant scattering and low coefficient of determination for a power-law regression ($H_{max} = 0.0255L^{1.0038}$, $R^2 = 0.47$). Cartwright et al. (1995) also found significant data scattering when analyzing the ratio between maximum vertical displacement and length of normal faults in the grabens of the Canyonlands, Utah. In a later study, Grosfils et al. (2003) indicated that Cartwright et al. (1995) underestimated the displacement to length relationships by assuming a limited thickness for the graben fill. The average aspect ratio derived from the two downhill-facing scarps associated with master faults is 0.05, i.e., almost twice as high as the value calculated for the uphill-facing scarps. Gutiérrez et al. (2012) calculated average aspect ratios of 0.008 and 0.02 for downhill-facing and uphill-facing scarps, respectively, in a graben generated by subsidence due to interstratal dissolution of evaporites (Iberian Range, NE Spain).

Collapse Structures and Grabens Related to Interstratal Dissolution of Evaporites in the Montcortés Lake Area

The structure of the Montcortés Lake area corresponds to an E-W–trending antiformal syncline with evaporitic Triassic sediments in the core, overlain by limestones of the older Muschelkalk facies (Fig. 3). The Triassic formations in the northern limb of the antiform are unconformably overlain by gently folded Paleogene conglomerates. Geological and geomorphological mapping reveals an ellipsoidal evaporite collapse area, 1.6 km in length, affecting the lower part of the Peracalç Range and Montcortés Lake area (Figs. 3 and 5). The boundary of this internally drained area of subsidence, including Montcortés Lake, is defined by arcuate scarps (Fig. 9A). In the northern sector of the collapse area, there is an ENE-WSW–trending graben that is 1450 m long and up to 630 m wide.

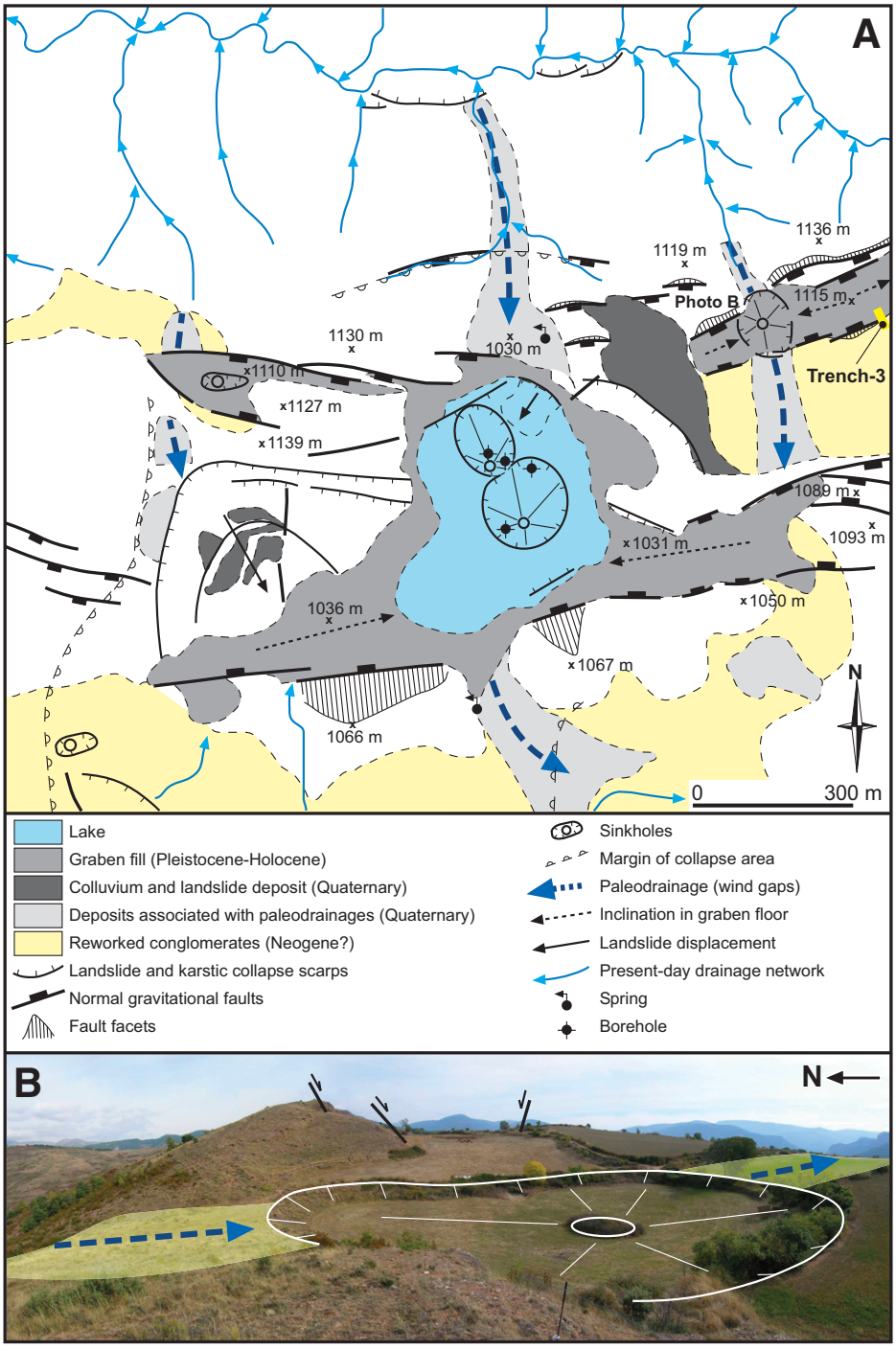

Figure 9. (A) Morphostructural map of Montcortés Lake area. See Figure 5 for location. The geomorphic features mapped in Montcortés Lake were derived from the lake bathymetry of Corella et al. (2011). (B) Paleodrainage disrupted by the northeastern secondary graben and a nested collapse sinkhole.

Secondary graben depressions with conspicuous geomorphic expression occur on both sides of this structure. The fault scarp at the southern margin of the graben displays conspicuous facets on ophites 25–30 m high. The bottom of the northern secondary grabens is affected by scarp-edged and subcircular collapse sinkholes.

Trench 3 was excavated across the southern fault scarp of the northeastern secondary graben (Fig. 9A). The mapped graben structure is related to the collapse of the crest of an antiform due to interstratal karstification of the evaporites forming its core. Similar graben structures, although tens of kilometers long, have been developed in the salt anticlines of the Paradox Basin, Utah and Colorado, in which cores consist of salt walls up to 4 km high (Cater, 1970; Doelling, 2000; Gutiérrez, 2004). In northern Michigan, Black (1997) reported graben valleys around 0.5 km wide generated by interstratal dissolution of gypsum controlled by preexisting tectonic fault and joints. Similar features (Heuschkel Park sag, Spring Valley structure) have been also identified in the Carbondale collapse center, Rocky Mountains, Colorado (Kirkham et al., 2002). Gutiérrez et al. (2012) investigated a 1.7-km-long graben in the Iberian Range, NE Spain, formed in the crest of a monocline generated by sagging due to karstification of subjacent Triassic evaporites.

Bathymetric surveys (Corella et al., 2011) reveal that Montcortés Lake, 525 m long and 30 m deep, corresponds to a karstic depression resulting from the coalescence of several collapse sinkholes. The arcuate scarps situated NE of the lake and crosscutting the secondary graben indicate that Montcortés Lake is the bottom of a larger collapse structure controlled by complex ring faulting, and that it is younger than the graben on which it is superimposed. Corella et al. (2011), in cores retrieved from the meromictic Montcortés Lake, inferred three major phases of landsliding that occurred around 1010, 1600, and 6000 cal. yr B.P. These subaqueous landslides were probably induced by undermining and loss of basal support related to dissolution-induced collapse events. The graben system has distorted a preexisting N-S drainage. The northeastern secondary graben east of Montcortés Lake has downfaulted sections of a S-directed paleostream, leaving a perched paleovalley in between (Fig. 9B). The coincidence of a collapse sinkhole in the NE graben floor with the trace of this paleodrainage may be related to more karstification below a former local base level and higher infiltration in the lowest point of an internally drained area. The graben and the large collapse structure have also disrupted the N-S drainage that used to flow along the Montcortés Lake area. Moreover, the northwestern secondary graben also has faulted a S-heading stream. In the bottom of this graben, there is also a collapse sinkhole.

TRENCHING AND ERT

Selection of Trench Sites

The locations of the three trenches excavated across gravitational faults, which subsequently determined the distribution of the three ERT profiles, were based on the following criteria: (1) accessibility, i.e., some favorable sites were discarded because they were not accessible even

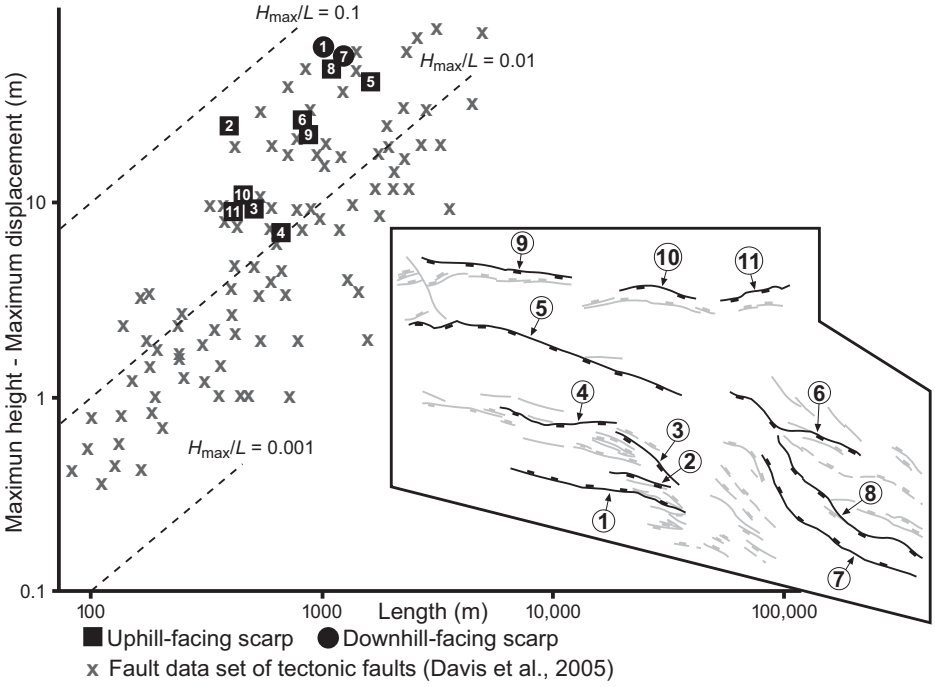

Figure 10. Log-log plot illustrating the relationship (aspect ratio) between the maximum height of downhill- and uphill-facing fault scarps and their length, measured as a straight line, in the lateral spread of Peracalç. Inset map shows the measured gravitational faults. Crosses correspond to maximum displacement and fault length data of tectonic faults including the global data set (Schlische et al., 1996) and data from the Ostler fault zone, New Zealand (Davis et al., 2005).

with a trackhoe; (2) datable material (high fault scarps with thick and nondatable coarse-grained colluvium at the foot were avoided), e.g., trench 1 was dug in a flat surface next to a fault scarp and trench 3 near the tip of a fault scarp; (3) sites where the topography and the texture of surface deposits suggested the presence of fine-grained facies including charcoal and organic sediments (the selection of the site for trench 2 was motivated by the presence of a small flood-prone closed depression at the foot of the scarp, which turned out to be an artificial excavation); (4) the possibility of finding faulted and datable correlative deposits on both sides of the fault (trench 1), which would allow calculating more precisely slip rates; and (5) logistics, i.e., priority was given to sites devoid of trees and where the acquisition of permits in a reasonable time frame was feasible.

Trench Site 1

A 128-m-long ERT profile (ERT 1) was acquired in a nearly flat depression related to a paleodrainage at the eastern sector of graben I (Fig. 6). The geoelectrical profile, with a N010E orientation, was sited across an antithetic fault scarp (N145E) on exposed limestone and traversing the eastward projection of another antislope fault scarp (Fig. 7A). The trace of the ERT 1 profile overlaps the location of trench 1, excavated across the projected trace of the southern N105N-striking fault. Highly resistive limestone bedrock of the Senyús Formation (ρ >350 Ωm) and low-resistivity Quaternary detrital cover (ρ <350 Ωm) may be differentiated in the ERT 1 profile (Fig. 11A). The spatial relationships between the two resistivity units allow us to infer a concealed graben, ~50 m wide, in which the cover deposits may reach 5–10 m in thickness. This interpretation is in agreement with the morphostructural map, showing a graben structure to the west of the profile. The S-dipping fault controlling this graben was exposed in trench 1. At the site of the northern fault scarp, the ERT profile reveals Quaternary deposits juxtaposed against bedrock.

Trench 1, around 21 m long and 2.3 m deep, exposed the concealed S-dipping fault interpreted in the ERT 1 profile (Fig. 11B). The limestone bedrock of the Senyús Formation displayed a very irregular pinnacled rockhead locally coated with cohesive red clay corresponding to a karstic residue. Two sedimentary packages can be differentiated in the cover deposits. The older units (2 and 3) are offset by the normal fault and restricted to the downthrown block. The undeformed younger units (4 and 5) extend across the whole trench and truncate the normal fault. Unit 2 consists of massive reddish-brown silty clay with matrix-supported subangular pebble- and granule-gravel with chaotic fabrics. This clastic unit is interpreted as a debris-flow facies. Unit 3 is brown massive sandy clay with scattered granule- and pebble-sized clasts and small gravel channels. This unit records low-energy water flows. Charcoal collected 110–120 cm above the base of the unit has yielded an age of 2140–1987 cal. yr B.P. at 2σ (Table 2). Unit 4 is made up of stratified subrounded and well-sorted loose granule- and pebble-gravel. The channeled base of this unit truncates the normal fault (event horizon) and units 3 and 2 in the downthrown block. The southern channel seems to be related to a longitudinal drainage developed along the axis of the graben situated to the west (Figs. 6 and 7), and its location is probably controlled by the concealed graben inferred from the ERT 1 profile. A 139–30 cal. yr B.P. age was obtained from a charcoal sample collected 10 cm above the base of this unit. Unit 5 consists of massive brown silty sand with subangular pebble-gravel. The upper 30-cm-thick part of this unit is highly disturbed by ploughing and shows a darker color. The fault exposed in the northern sector of the trench, with a 57°S dip, juxtaposes the massive units 2 and 3 against highly brecciated bedrock with shear fabrics. The lower part of unit 2 seems to fill a 50-cm-wide fissure associated with the fault. This fissure together with the low dip of the fault suggest a significant horizontal displacement component, with resulting heave and dilation. In the east side of the trench, unit 3 next to the fault shows clasts with reoriented fabrics subparallel to the failure plane.

The stratigraphic and structural relationships observed in the trench record a minimum of one displacement event on the exposed fault, which occurred between deposition of units 3 and 4 (Fig. 11C). The available numerical ages provide a poorly constrained age of 2.0–0.1 ka for this faulting event. The stick-slip displacement style inferred for this gravitational fault is coherent with the compound scarp associated with this structure to the west, showing an upper beveled and degraded segment and a steep and fresh-looking younger segment. These features are characteristic of fault scarps that undergo episodic rejuvenation (e.g., McCalpin, 2009b). Assuming that unit 3 was deposited on both sides of the fault, as suggested by its sedimentological characteristics, its thickness between stations 16 and 17 provides a minimum estimate for the vertical offset of 100 cm. Unit 2 is not taken into account because it is discontinuous (locally interrupted by bedrock). Considering a maximum age of

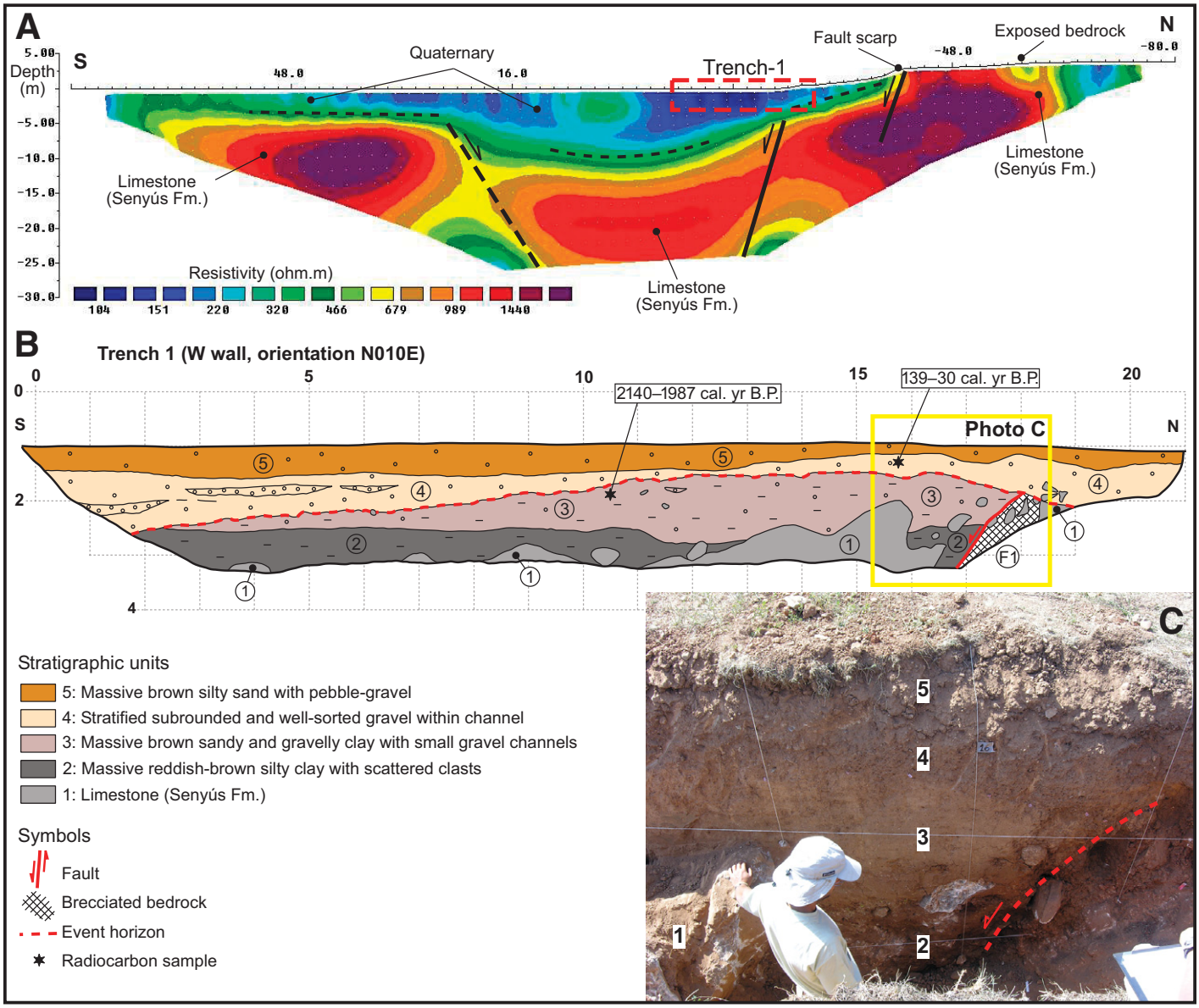

Figure 11. (A) Profile ERT-1 acquired in the eastern sector of graben I (scale in meters). See location in Figure 7. (B) Trench 1 excavated across the projection of a compound antithetic fault scarp. See location in Figures 6 and 7. (C) Image of the fault zone (dashed red line) exposed on the W side of the trench 1. The left hand of the person rests on a limestone pinnacle. ERT—electric resistivity tomography.

2.0 ka for the faulting event and a minimum vertical separation of 100 cm, we can calculate a minimum apparent vertical slip rate of 0.5 mm/yr. Following McCalpin (2009c), we use the term apparent because the slip rate has not been estimated for closed slip cycles (McCalpin, 2009c). The actual value may be significantly higher because we use a maximum age and a minimum displacement. Moreover, this apparent slip rate is obtained close to the tip of the fault. Much higher rates can be expected at the central sector of the structure, where the displacement-per-event values are generally higher.

Trench Site 2

This site is located in the western sector of the intermediate graben III. Trench 2 was excavated across the northern antithetic fault scarp (Fig. 6). The ERT 2b profile, 400 m long, was acquired along the graben axis and centered at the intersection with profile ERT 2b and trench 2. The contrast between the high-resistivity calcareous bedrock of the Senyús Formation and the more conductive graben fill in profile ERT 2a allows us to estimate an approximate thickness of 40 m for the latter (Fig. 12A). The high-resistivity upper unit of the western sector of the profile corresponds to a mapped landslide deposit, made up of brecciated limestone superimposed on the finer-grained graben fill (Fig. 6). The ERT 2a profile, 150 m long, was obtained perpendicular to the trenched fault scarp and next to the site of trench 2. It clearly captures the S-dipping fault that juxtaposes the high-resistivity (ρ >350 Ωm) limestone bedrock underlying the upper part of the scarp against the more conductive Quaternary graben fill (Fig. 12B). Unfortunately, this fault was not exposed in trench 2 because it was beyond the maximum range of the backhoe.

The 18-m-long and 2.1-m-deep trench 2 was excavated across the 8-m-high antithetic

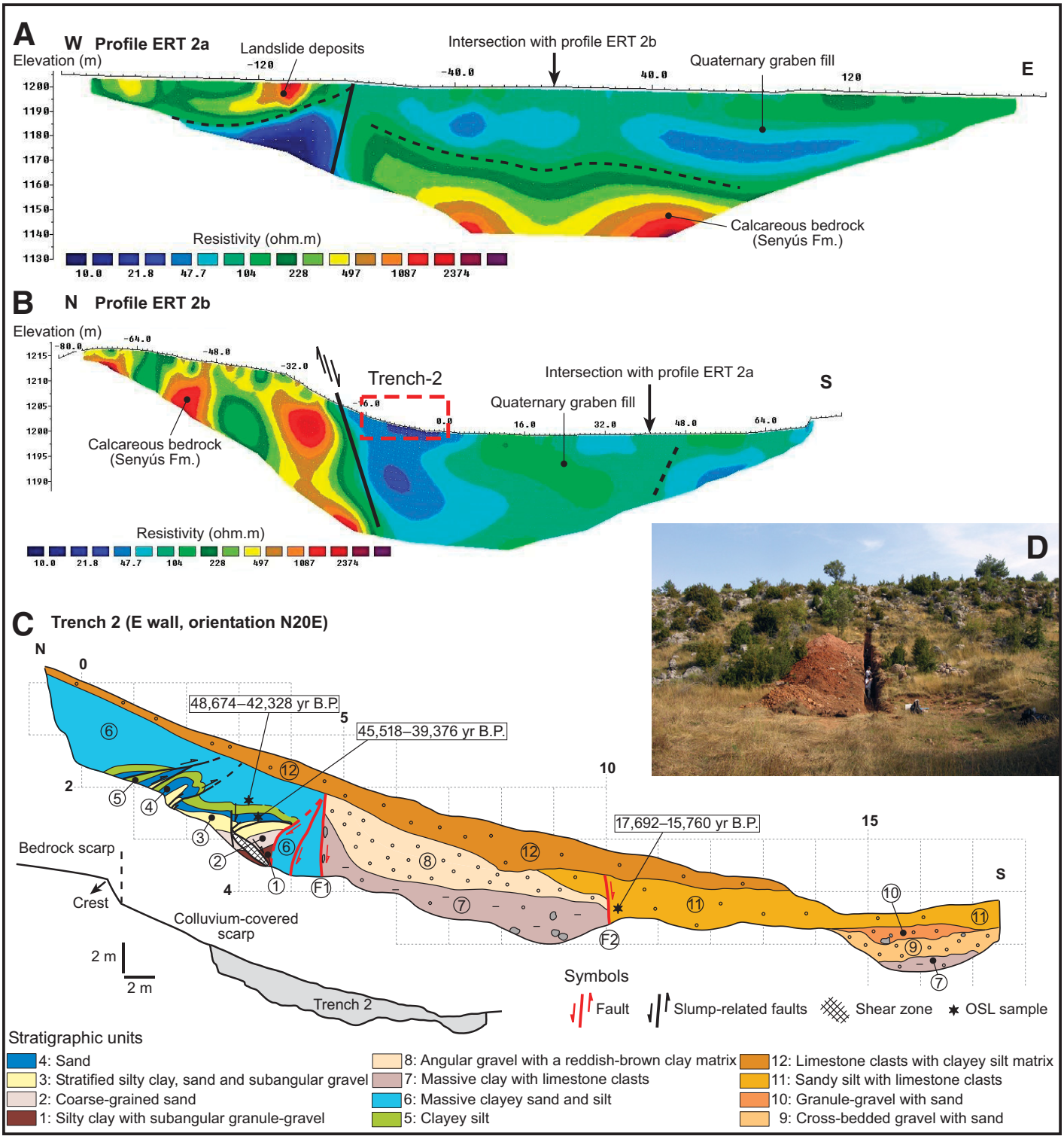

Figure 12. Electrical resistivity tomography (ERT) profiles (A) ERT 2a (longitudinal) and (B) ERT 2b (transverse) acquired in trench site 2. (C) Log of trench 2 and topographic profile of the scarp. (D) Photograph of trench 2. OSL—optically stimulated luminescence.

fault scarp, in which limestone bedrock was exposed in the upper 1.9 m below the scarp crest (Figs. 12C and 12D). We expected to find a master fault juxtaposing coarse-grained colluvium against limestone bedrock in the intermediate sector of the scarp (McCalpin, 1987, 2009b). Conversely, the upward projection of this fault intersects the topography in the upper part of the scarp, and the finer-grained facies found in the trench were those located in the most proximal position (Fig. 12C).

The trench exposed multiple deformed stratigraphic units (units 1–11) affected by two main subvertical normal faults (F1 and F2) truncated by nondeformed colluvium (unit 12). The oldest stratigraphic units occur in the footwall of fault F1: (1) reddish-brown silty clay with scattered subangular granule-gravel; (2) brown well-sorted coarse-grained sand; (3) finely stratified and well-sorted orange and pale-purple silty clay and sand and subangular granule- pebble-gravel; (4) reddish-brown sand showing a fining-upward sequence; (5) pale-orange clayey silt; and (6) massive clayey sand and silt up to 1.8 m thick. The identification of folds and faults within this unit was highly difficult due to its fine texture and massive character. Samples collected from units 4 and 6 provided overlapping OSL age ranges of 45,518–39,376 yr B.P. and 48,674–42,328 yr B.P., respectively. The overlapping time interval, corresponding to the relatively warm and humid marine oxygen isotope stage (MIS) 3, may be considered a good age estimate for these deposits (45.5–42.3 ka). This sedimentary package is interpreted as lacustrine deposits accumulated in a paleolake developed within the graben. The fine-grained texture of these sediments, despite the proximity to the bedrock fault, suggests that during deposition of this sequence, the scarp was relatively small and/or covered by dense vegetation. The stratigraphic units N of fault F1 are affected by stacked S-verging folds and thrusts ascribable to the toe of a subaqueous landslide (slump) developed on soft, water-saturated and cohesive deposits (Martinsen, 1994). At station 4, two S-dipping normal faults with limited displacement are superimposed on the slump-related contractional structures. The first is a small-throw (6 cm), down-to-the-south, steep normal fault. This failure plane dies out in unit 5, in which the displacement is accommodated by a small monocline. This feature suggests that the fault developed soon after the slump when the deposits were still soft. The second is a normal fault with a 50°S dip connected with the former one and defined in the trench by a sheared lenticular horse. These structures may correspond to penecontemporaneous gravitational failures developed at the toe of the slumped mass, probably oversteepened and destabilized by the successive stacking and propagation of slide deposits. The two oversteepened normal faults situated S of the lenticular shear zone are probably secondary structures associated with fault F1. A minimum vertical displacement of 80 cm can be measured for the northern oversteepened fault. The vertical fault F1 juxtaposes unit 6 against units 7 and 8 in the downthrown block, which are affected by a drag fold and show clasts with reoriented fabrics. The thickness of units 7 and 8 next to the fault provides a minimum vertical displacement of 192 cm on this structure.

Two sedimentary packages can be differentiated S of fault F1, the apparently tabular units 7 and 8, and units 9, 10, and 11. The latter package fills a channel that truncates unit 8 and the axis of which seems to be located at the foot of the scarp. Unit 7 is reddish-brown massive clay with floating poorly sorted angular limestone clasts up to 15 cm long. Unit 8 is a roughly stratified, poorly sorted and angular pebble- and cobble-gravel with a reddish-brown clay matrix. Units 7 and 8 may be interpreted as sediment-gravity and water-flow deposits accumulated in the graben floor. Unit 9 is cross-bedded pebble-granule-gravel with sand matrix. Unit 10 consists of well-sorted granule-gravel with sand matrix. Unit 11 is roughly stratified sandy silt with scattered subangular limestone clasts. An OSL age of 17,692–15,760 yr B.P. was obtained from a sample collected in this unit next to fault F2. Units 9–11 were probably deposited in a channel running along the foot of the scarp. Unit 12 is the undeformed colluvium, made up of angular gravel- and boulder-sized limestone clasts with a brown clayey silt matrix.

Units 7 and 8 show drag folds next to faults F1 and F2. Downward flexure within this block accounts for a vertical displacement of 190 cm, assuming that the contact between both units was originally horizontal. A minimum vertical separation of 46 cm can be measured on fault F2. Overall, the stratigraphic and structural relationships of the trench indicate episodic faulting, whereby the sequential development of new faults toward the graben caused the relative uplift of graben deposits favoring the development of slumps, the basinward migration of the depositional axis, and recycling of the upthrown graben sediments. This latter circumstance limits the preservation potential of colluvial wedges, since deposits accumulated at the foot of the scarp become part of a new rejuvenated scarp after subsequent forward faulting (Gutiérrez et al., 2009). The formation of the investigated graben, with a sedimentary fill ~40 m thick, must have been achieved through many faulting events, probably in combination with creeping subsidence. The geometric relationships observed in the trench may be explained with a minimum of three to four faulting events. At least one faulting event older than 45.5–42.3 ka is required in order to have created the lake in which units 1–6 were deposited. The basinward verging contractional structures affecting the lacustrine sequence most likely record another faulting event, which oversteepened the lake bed and triggered slumping. The superimposed S-dipping normal faults are probably penecontemporaneous gravitational failures developed at the toe of the slide mass (Martinsen, 1994, and references therein). Slumping most likely occurred soon after deposition of the lake sediments, around 45.5–42.3 ka. Fault system F1 and fault F2 may have formed in a single faulting event. However, the episodic basinward displacement of the graben floor suggested by the offlapping units 7–8 and 9–11 supports the alternative of two different events. Fault F1 would be younger than 45.5–42.3 ka, and fault F2 would be younger than 17.6–15.7 ka. The minimum cumulative vertical displacement measured in the trench (508 cm) and the maximum age for this deformation (45.5 ka) yield a minimum apparent vertical slip rate of 0.1 mm/yr. The actual value must be much larger, since the total amount of deformation is not well known, and its age is very poorly constrained.

Trench Site 3

Trench 3 was excavated across the N-facing scarp defining the S margin of the northeastern secondary graben in Moncortés Lake area. Here, Oligocene conglomerates unconformably overlie the northern limb of the evaporite-cored Bellera antiform. The trench, 10 m long and 1.9 m deep, was excavated in a crop field near the eastern tip of a 110-m-long fault scarp, around 2 m high at the trench site and clearly degraded by agricultural activity.

Two main units made up of stratified gravels were exposed in the trench on both sides of the N-dipping normal fault F1, which is considered to be the master fault (Fig. 13). Unit 1, in the footwall of fault F1, is brown stratified, subrounded, polymictic, and cemented Oligocene pebble-cobble-gravel. Unit 2, in the hanging wall of fault F1, is made up of loose, stratified, rounded, and polymictic gravel and abundant secondary carbonate. Unit 2 has a finer texture and a lighter-brown color than unit 1. Fault F1 shows a 25-cm-wide shear zone consisting of gravels with reoriented fabrics. Fault F2 is associated with a 28-cm-wide fissure filled with reddish-brown clay and scattered rounded gravels. The gravels in the wedge-shaped body between the fault and the fissure show obvious shear fabrics. Fault F3 is defined by an 80-cm-wide zone of dilated and sheared gravels with reoriented

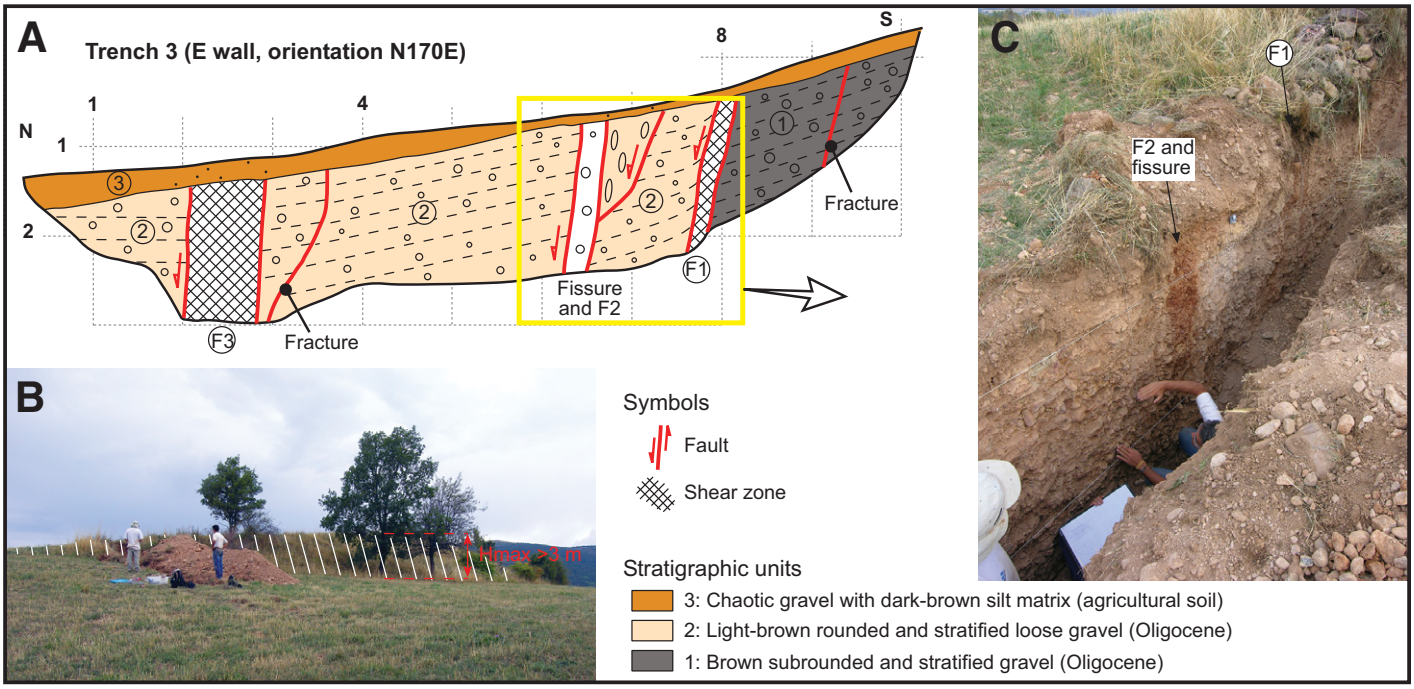

Figure 13. (A) Log of trench 3 excavated across a scarp at the S margin of the northeastern graben in the Montcortés Lake area. See location in Figure 9. (B) Image showing the trench near the eastern tip of the scarp, degraded by agricultural activity. (C) Photograph of the logged side of the trench where faults F1 and F2, and the associated fissure were recognized.

fabrics and abundant soil-derived pale-brown silty clay matrix with secondary carbonate. Unit 1 shows an apparent horizontal dip in the footwall of fault F3, whereas gravels of unit 1 and 2 of this fault have a persistent 10N dip. South of faults F1 and F3, we also mapped N-dipping fractures filled with downward percolated reddish silty clay. All the structures are truncated by a contemporaneous agricultural soil disturbed by ploughing (unit 3), a massive poorly sorted chaotic gravel with dark-brown silt matrix. The structures exposed in the trench demonstrate that the trenched scarp is not erosional but is related to faulting and northward tilting resulting from evaporite dissolution at depth. Moreover, the presence of fissures and dilated gravels indicates significant horizontal extension. Probably, this extension counterbalances the shortening in the central sector of the graben due to a subsidence component accommodated by passive bending (sagging) of the conglomerates (i.e., Gutiérrez et al., 2008, 2012).

Unfortunately, the exposed geometric relationships and the lack of distinguishable stratigraphic markers in the trenched units precluded the possibility of elucidating the kinematic regime of the structures (episodic vs. continuous) and measuring any vertical displacement on the faults. Probably, extending the trench toward the central sector of the graben, where the presence of datable fine-grained facies is more likely, would have allowed us to obtain more information. However, the length of the trench was limited by permit constraints.

DISCUSSION AND CONCLUSIONS

In the laterally unconfined Peracalç Range, with a local relief of around 450 m, the thick (~2.5 km) halite-bearing argillaceous Triassic sediments, overlain by a carbonate and conglomerate sequence 250 m thick, have expanded outward, generating a bulge at the foot of the range. Lateral extension has been accommodated in the overlying brittle sequence through the development of a prominent horst and graben morphostructure covering around 4.5 km^2. Two main mechanisms may have been involved in the lateral migration of the Triassic clays and evaporites favored by differential loading: (1) ductile deformation of argillaceous sediments toward the laterally debuttressed front of the range, and (2) halokinetic flow of the halite-bearing evaporites toward the unloaded foot of the range (i.e., Huntoon, 1982; Simpson, 2004; Lucha et al., 2012). The horst and graben structure also shows a significant vertical displacement attributable to subsidence caused by interstratal karstification of evaporites. This interpretation is supported by the presence of grabens and collapse structures caused by evaporite dissolution in the erosional depression situated at the foot of the range, together with major saline springs in the adjacent Noguera-Pallaresa River valley. The lack of deep subsurface data precludes testing the hypotheses proposed about the mechanisms involved in the gravitational slope deformation. Deep boreholes equipped with inclinometers would allow us to obtain quantitative information on the contribution of the different deformation components to the overall displacement, their distribution at depth, and their short-term temporal variability.

A minimum volume of 0.9 km^3 has been estimated for this active lateral spread, excluding the unknown thickness of Triassic clays and evaporites involved in the gravitational deformation. This is to our knowledge the largest landslide documented in the Pyrenees. The graben depressions, up to 1.7 km long and 400 m wide, are bounded by low-sinuosity downhill- and uphill-facing scarps controlled by synthetic and antithetic faults with en echelon arrangement. These normal faults, with prevalent ENE-WSW to NW-SE strikes, seem to have been guided by the preexisting tectonic structure, largely related to the underlying Morreres back thrust. Obvious accommodation ramps can be observed in the stepovers associated with overlapping fault segments. The development of horsts and grabens has deformed and aborted a former N- to NE-directed paleodrainage, recognizable as wind gaps in the upper part of the horsts, hanging

valleys in downhill-facing scarps, and closed depressions associated with streams defeated by antislope scarps.

The following factors have favored the development of the Peracalç Range lateral spread: (1) Thick soluble and ductile halite-bearing Triassic sediments are overlain by a brittle carbonate sequence affected by tectonic faults subparallel to the range front. The Triassic sediments are susceptible to ductile deformation, halokinesis, and rapid dissolution. (2) Lateral debuttressing and unloading of the Mesozoic sediments formed the Peracalç Range, once covered by a thick Oligocene sequence of conglomerates. Considering an overburden thickness of 450 m and a minimum density of 2 g/cm^3, we can estimate a stress release due to differential erosion at the foot of Peracalç Range of ~9 MPa. (3) Massive amounts of water infiltrated through tensile fissures in the lateral spread, dominated by internal drainage. The incorporation of water contributes to reduce the mechanical strength of the Triassic formation by increasing the water content in the clayey sediments and rapidly dissolving the evaporites (Tran et al., 2011; Gutiérrez and Cooper, 2012). (4) There is evidence of loss of basal support and subsidence due to dissolution of evaporites within the Peracalç Range and at its foot.

The oldest numerical age obtained from the trenched graben deposits provides a minimum age of 45 ka for the lateral spread of Peracalç Range. Several lines of evidence indicate that this landslide has evolved retrogressively and that the highest rate of differential deformation is currently occurring in the head sector: (1) The upper graben system shows the largest and more fresh-looking open fissures, as well as the scarps with the lowest degree of degradation. (2) The infill of graben III, situated in an intermediate position, may reach 40 m, whereas the upper graben is largely devoid of sedimentary fill. (3) Fault segments show a higher degree of hard-linkage, suggesting an older age. (4) The drainage network in the upper part of the lateral spread is completely disrupted, whereas in the lower graben, there has been some adjustment between the new streams governed by the grabens and the preexisting transverse drainages.

According to our calculations, the horizontal separation (heave) related to dip-slip displacement on normal faults in the lateral spread of Peracalç has accommodated a cumulative extension of around 42–138 m. Considering this deformation range, which excludes the dilation component on faults and fissures, and the minimum age of the slope movement (45 ka), we can tentatively estimate an average long-term horizontal displacement rate of 0.94–3.06 mm/yr. The active slope movement of Peracalç, with extensive bedrock exposure, offers excellent opportunities to investigate the kinematics of a large rock spread involving evaporite dissolution, using geodetic techniques such as GPS and DInSAR. The latter technique may provide average displacement rates and deformation time series with a high spatial resolution and accuracy, allowing the analysis of the spatial and temporal variability of the ground deformation (i.e., Furuya et al., 2007).

Average maximum height to length ratios (H_{max}/L) of 0.05 and 0.029 have been calculated for a limited number of downhill-facing and uphill-facing scarps in the lateral spread of Peracalç Range, respectively. The higher aspect ratios obtained for the downhill-facing scarps are most likely related to the larger throw on the synthetic master faults, which accommodate most of the vertical displacement. Grosfils et al. (2003) calculated a maximum displacement to fault length ratios (D_{max}/L) ratio of 0.045 for the master fault of Devils Lane graben (graben of Canyonlands, Utah), the only structure of this large-scale lateral spread for which information on the graben-fill thickness was available. Dawers et al. (1993), using data from Quaternary normal fault scarps in the Volcanic Tableland, California, and including faults for which lengths spanned three orders of magnitude, estimated maximum D_{max}/L of the order of 0.01. A similar D_{max}/L relationship is found for short faults (10–1000 m) combining several data sets (Cowie and Scholz, 1992; Schlische et al., 1996; Davis et al., 2005). The H_{max}/L ratios obtained for the scarps of the Peracalç lateral spread, which are a minimum estimate for the D_{max}/L ratio (aggradation and erosion in the footwall and hanging wall, respectively), suggest that gravitational fault scarps in lateral spreads tend to have higher aspect ratios than tectonic faults. For instance, fault scarp number 5 has a maximum height of 42 m. However, the maximum displacement on this fault is greater than 80 m, considering that the graben fill reaches at least 40 m, as indicated by the ERT profiles; i.e., D_{max}/L is twice as high as the H_{max}/L ratio. A similar finding was presented by Gutiérrez et al. (2012) analyzing fault scarps associated with a graben generated by interstratal dissolution of evaporites in the Iberian Range, Spain. The high aspect ratios of the investigated fault scarps may be related to two circumstances: (1) Vertical displacement on these faults is significantly higher than on tectonic faults of comparable length due to subsidence caused by interstratal karstification of the evaporites underlying the brittle plate. (2) These faults are gravitational structures merely a few hundred meters deep, whereas tectonic faults may go through the whole seismogenic crust. Several studies report on the higher aspect ratios of gravitational fault scarps compared to those of tectonic origin including sackung (McCalpin, 1999), landslides (Cotton, 1999), and faults scarps generated by evaporite dissolution collapse (Gutiérrez et al., 2012). On the other hand, the apparent vertical slip inferred from trench 1 (>0.5 mm/yr) suggests that gravitational faults may reach significantly higher displacement rates than tectonic faults in the investigated geotectonic setting (i.e., Ortuño et al., 2008). These criteria may be useful to elucidate whether active fault scarps correspond to tectonic structures (seismogenic) or to gravitational failures (nonseismogenic). Hell Creek fault, British Columbia, Canada, illustrates the relevance of this dilemma. This fault with prominent geomorphic expression is considered by the provincial utility (BC Hydro) to be the main seismogenic fault that could impact the Terzaghi Dam (McCleary et al., 1978; Ertec, 1981), whereas the Geological Survey of Canada attributes this controversial structure to nonseismic gravity failure (Clague and Evans, 1994).

Lateral spreads are generally assumed to be extremely slow slope movements characterized by progressive displacement. However, the geometric relationships observed in trenches 1 and 2 provide evidence for episodic displacement. In trench 2, we have inferred a minimum of three to four faulting events, one of them recorded by the development of subaqueous slumps in lake deposits at around 45–42 ka. A recent faulting event has been identified in trench 1, the poorly constrained age (2.0–0.1 ka) of which overlaps the timing of the two most recent landsliding phases identified in Montcortés Lake deposits (Corella et al., 2011). The unexpected stick-slip kinematic behavior of this deep-seated slope movement may be related to subsidence caused by interstratal dissolution of the underlying halite-bearing evaporites. Although dissolution by groundwater flow operates in a continuous fashion, subsidence through brittle collapse may be a stepwise process occurring when the lack of basal support generated by karstification reaches a stability threshold. Dissolution processes may be enhanced by higher groundwater recharge due to higher precipitation and/or higher infiltration induced by surface faulting and fissuring. It may also increase due to erosional base-level lowering, involving an increase in the hydraulic gradient and favoring the deepening of groundwater flows. On the other hand, gravitational faulting events may be also triggered by seismic shaking. The Pyrenees is one of the most seismically active areas in Western Europe (Nicolas et al., 1990) and has been the site of destructive earthquakes in the past (e.g., Susagna et al., 1994; Olivera et al., 2006; Dubos- Sallée et al., 2007), some of them with M_w >6. However, the

poorly constrained chronology of the inferred displacement events and the lack of numerically dated paleoseismic records in the area preclude exploration of this hypothesis.

An ellipsoidal evaporite collapse area, 1.6 km long, has been identified at the foot of Peracalç Range, affecting one of the lowest grabens of the lateral spread. Moreover, a complex 1.4-km-long graben with conspicuous fault scarps has been mapped in the Montcortés Lake area. This graben resulted from the collapse of the crest of the Bellera antiform, as a result of interstratal karstification of the halite-bearing evaporites of its core. Similar structures, but with a much larger scale, have been documented in the salt anticlines of Canyonlands, Utah and Colorado (Cater, 1970; Doelling, 2000; Gutiérrez, 2004). These graben depressions with nested collapse sinkholes have deformed and aborted a paleodrainage, expressed as wind gaps. The evaporite dissolution-collapse structures mapped at the foot of Peracalç Range support the idea that subsidence due to interstratal evaporite karstification plays a significant role in the development of the Peracalç lateral spread.

The study area, situated astride two major structural units of the Pyrenees bounded by the Morreres back thrust, has received disparate tectonic interpretations that overlook the gravitational faults of the large Peracalç rock spread (García Senz, 2002; Saura, 2004). In previous works, the grabens were erroneously interpreted as erosional strike depressions carved in less resistant marls. This case study suggests that, when making geological maps in mountainous regions, it is highly advisable to incorporate the concept of large deep-seated slope movements. For example, the revision of the Climax 7.5′ quadrangle in the Rocky Mountains of Colorado by a trained geomorphologist demonstrated that large landslides cover an area seven times larger than in the previous map, representing 9.5% of the quadrangle (McCalpin, 2008). Similarly, Gutiérrez et al. (2011), mapping a large area in the Pyrenees where deep-seated landslides represent around 20% of the area, demonstrated that a considerable proportion of the faults and strike and dip data of the geological map are related to postglacial deep-seated landslides, rather than to tectonic deformation.

ACKNOWLEDGMENTS

This research work was funded by the national projects CGL2005-02404 and CGL2010-16775 (Ministerio de Ciencia e Innovación and Fondo Europeo de Desarrollo Regional [FEDER]). The authors are very grateful to P. Lucha and G. Rivas for their assistance during the trenching campaigns. The article was improved thanks to the insightful comments of Eric Kirby, Karl Mueller, and an anonymous reviewer.

REFERENCES CITED

Alves, T.M., and Lourenço, S.D.N., 2010, Geomorphic features related to gravitational collapse: Submarine landsliding to lateral spreading on a late Miocene–Quaternary slope (SE Crete, eastern Mediterranean): Geomorphology, v. 123, p. 13–33, doi:10.1016/j.geomorph.2010.04.030.

Baars, D.L., 2000, Geology of Canyonlands National Park, Utah, *in* Sprinkel, D.A., Chidsey, T.C., and Anderson, P.B., eds., Geology of Utah's Parks and Monuments: Utah Geological Association Publication 28, p. 61–83.

Beamud, E., Muñoz, J.M., Fitzgerald, P.G., Baldwin, S.L., Garcés, M., Cabrera, Ll., and Metcalfz, J.R., 2011, Magnetostratigraphy and detrital apatite fission track thermochronology in syntectonic conglomerates: Constraints on the exhumation of the south-central Pyrenees: Basin Research, v. 23, p. 309–331, doi:10.1111/j.1365-2117.2010.00492.x.

Berástegui, X., García-Senz, J.M., and Losantos, M., 1990, Tecto-sedimentary evolution of the Organyà extensional basin (central south Pyrenean unit, Spain) during the Lower Cretaceous: Bulletin de la Société Géologique de France, v. 6, no. 2, p. 251–264.

Berástegui, X., Losantos, M., Muñoz, J.A., and Puigdefábregas, C., 1993, Tall Geològic del Pirineu Central 1:200,000: Barcelona, Spain, Servicio Geológico de Cataluña e Instituto Cartográfico de Cataluna (SGC-ICC), 62 p., 1 sheet.

Bernaus, J.M., Caus, E., and Arnaud-Vanneau, A., 2000, Aplicación de los análisis micropaleontológicos cuantitativos en estratigrafía secuencial: El Cretácio inferior de la cuenca de Organyà (Pirineos España): Revista de la Sociedad Geológica de España, v. 13, no. 1, p. 53–63.

Biggar, N.E., and Adams, J.A., 1987, Dates derived from Quaternary strata in the vicinity of Canyonlands National Park, *in* Campbell, J.A., ed., Geology of Cataract Canyon and Vicinity: Salt Lake City, Utah, Four Corners Geological Society, 10th Field Conference Guidebook, p. 127–136.

Black, T.J., 1997, Evaporite karst of northern Lower Michigan: Carbonates and Evaporites, v. 12, p. 81–83, doi:10.1007/BF03175805.

Bordonau, J., 1992, Els Complexos Glacio-Lacustres Relacionats amb el Darrer Cicle Glacial als Pirineus: Logroño, Spain, Geoforma, 251 p.

Bru, J., Martí, J., Ventura, J., and Vilaplana, J.M., 1994, Geomorfología glaciar del Pirineo central, *in* Martí-Bono, C., and García-Ruiz, J.M., eds., El Glaciarismo Surpirenaico: Nuevas Aportaciones: Logroño, Spain, Geoforma, Map, scale 1:50,000.

Calvet, F., Anglada, E., and Salvany, J.M., 2004, El Triásico de los Pirineos, *in* Vera, J.A., ed., Geología de España: Madrid, Spain, Sociedad Española de Geomorfología-Instituto Geológico y Minero de España (SGE-IGME), p. 272–274.

Cancelli, A., and Pellegrini, M., 1987, Deep-seated gravitational deformations in the Northern Apennines, Italy: Proceeding 5th International Conference and Field Workshop on Landslides, Australia and New Zealand, p. 1–8.

Canérot, J., Hudec, M.R., and Rockenbauch, K., 2005, Mesozoic diapirism in the Pyrenean orogen: Salt tectonics on a transform plate boundary: American Association of Petroleum Geologists Bulletin, v. 89, no. 2, p. 211–229, doi:10.1306/09170404007.

Carobene, L., and Cevasco, A., 2011, A large scale lateral spreading, its genesis and Quaternary evolution in the coastal sector between Cogoleto and Varezze (Liguria, Italy): Geomorphology, v. 129, p. 398–411, doi:10.1016/j.geomorph.2011.03.006.

Cartwright, J.A., and Mansfield, C.S., 1998, Lateral displacement variation and lateral tip geometry of normal faults in the Canyonlands National Park, Utah: Journal of Structural Geology, v. 20, no. 1, p. 3–19, doi:10.1016/S0191-8141(97)00079-5.

Cartwright, J.A., Trudgill, B.D., and Mansfield, C.S., 1995, Fault growth by segment linkage: An explanation for scatter in maximum displacement and trace length data from the Canyonlands grabens of SE Utah: Journal of Structural Geology, v. 17, p. 1319–1326, doi:10.1016/0191-8141(95)00033-A.

Cater, F., 1970, Geology of the Salt Anticline Region in Southwestern Colorado: U.S. Geological Survey Professional Paper 637, 80 p.

Cauchon-Voyer, G., Locat, J., Leroueil, S., St-Onge, G., and Demers, D., 2011, Large-scale subaerial and submarine Holocene and recent mass movements in the Betsiamites area, Quebec, Canada: Engineering Geology, v. 121, p. 28–45, doi:10.1016/j.enggeo.2011.04.011.

Choukroune, P., and ECORS Team, 1989, The ECORS Pyrenean deep seismic profile reflection data and the overall structure of an orogenic belt: Tectonics, v. 8, p. 23–39, doi:10.1029/TC008i001p00023.

Clague, J.J., and Evans, S.G., 1994, A gravitational origin for the Hell Creek "fault," British Columbia, *in* Current Research 1994-A: Ottawa, Geological Survey of Canada, p. 193–200.

Commins, D., Gupta, S., and Cartwright, J., 2005, Deformed streams reveal growth and linkage of a normal fault array in the Canyonlands graben, Utah: Geology, v. 33, no. 8, p. 645–648, doi:10.1130/G21433.1.

Conti, S., and Tosatti, G., 1996, Tectonic vs. gravitational processes affecting Ligurian and Epiligurian units in the Marecchia valley (Northern Apennines): Memorie di Scienze Geologiche, v. 48, p. 107–142.

Corella, J.P., Moreno, A., Morellón, M., Rull, V., Giralt, S., Rico, M.T., Pérez-Sanz, A., and Valero-Garcés, B., 2011, Climate and human impact on a meromictic lake during the last 6,000 years (Montcortès Lake, central Pyrenees, Spain): Journal of Paleolimnology, doi:10.1007/s10933-010-9443-3.

Cotton, W., 1999, Criteria for identifying nonseismogenic-nontectonic phenomena: Landslide faults, *in* Hanson, K.L., Kelson, K.I., Angell, M.A., and Lettis, W.R., eds., Techniques for Identifying Faults and Determining their Origins: Washington, D.C., U.S. Nuclear Regulatory Commission, p. 2.52–2.55.

Cowie, P.A., and Scholz, C.H., 1992, Displacement-length scaling relationship for faults: Data synthesis and discussion: Journal of Structural Geology, v. 14, p. 1149–1156, doi:10.1016/0191-8141(92)90066-6.

Cruden, D.M., and Varnes, D.J., 1996, Landslide types and processes, *in* Turner, A.K., and Schuster, R.L., eds., Landslides: Investigation and Mitigation: Transportation Research Board, National Research Council, Special Report 247, p. 36–75.

Davis, K., Burbank, D.W., Fisher, D., Wallace, S., and Nobes, D., 2005, Thrust-fault growth and segment linkage in the active Ostler fault zone, New Zealand: Journal of Structural Geology, v. 27, p. 1528–1546, doi:10.1016/j.jsg.2005.04.011.

Dawers, N.H., Anders, M.H., and Scholz, C.H., 1993, Growth of normal faults: Displacement-length scaling: Geology, v. 21, p. 1107–1110, doi:10.1130/0091-7613(1993)021<1107:GONFDL>2.3.CO;2.

Delgado, J., Vicente, F., García-Tortosa, F., Alfaro, P., Estévez, A., López-Sánchez, J.M., Tomás, R., and Mallorquí, J.J., 2011, A deep seated compound rotational rock slide and rock spreads in SE Spain: Structural control and DInSAR monitoring: Geomorphology, v. 129, p. 252–262, doi:10.1016/j.geomorph.2011.02.019.

Diegel, F.A., Karlo, J.F., Schuster, D.C., Shoup, R.C., and Tauvers, P.R., 1995, Cenozoic structural evolution and tectono-stratigraphic framework of the northern Gulf Coast continental margin, *in* Jackson, M.P.A., Roberts, D.G., and Snelson, S., eds., Salt Tectonics: A Global Perspective: American Association of Petroleum Geologists Memoir 65, p. 109–151.

Doelling, H.H., 2000, Geology of Arches National Park, Grand Country, Utah, *in* Sprinkel, D.A., Chidsey, T.C., and Anderson, P.B., eds., Geology of Utah's Parks and Monuments, Volume 28: Salt Lake City, Utah, Utah Geological Association, p. 11–36.

Dubos-Sallée, N., Nivière, B., Lacan, P., and Hervouët, Y., 2007, A structural model for the seismicity of the Arudy (1980) epicentral area (western Pyrenees, France): Geophysical Journal International, v. 171, no. 1, p. 259–270, doi:10.1111/j.1365-246X.2007.03499.x.

Ely, R.W., 1987, Colluvium-filled fault fissures in the Needles fault zone, Cataract Canyon, Utah, *in* Campbell, J.A., ed., Geology of Cataract Canyon and Vicinity: Salt Lake City, Utah, Four Corners Geological Society, 10th Field Conference Guidebook, p. 69–73.

Ertec Northwest, Inc., 1981, The Origins(s) of Uphill-Facing Scarps, North Cascade Range, Washington: Seattle, Washington, Report by Ertec Northwest, Inc., submitted to Puget Sound Power and Light Co., November 1981, Report No. 81-513, 77 p.

Fossen, H., Schultz, R.A., Rundhovde, E., Rotevatn, A., and Buckley, S.J., 2010, Fault linkage and graben stepovers in the Canyonlands (Utah) and the North Sea Viking graben, with implications for hydrocarbon migration and accumulation: American Association of Petroleum Geologists Bulletin, v. 94, no. 5, p. 597–613, doi:10.1306/10130909088.

Furuya, M., Mueller, K., and Wahr, J., 2007, Active salt tectonics in the Needles District, Canyonlands (Utah), as detected by interferometric synthetic aperture radar and point target analysis: 1992–2002: Journal of Geophysical Research–Solid Earth, v. 112, B06418, doi:10.1029/2006JB004302.

García Senz, J., 2002, Cuencas Extensivas del Cretácico Inferior en los Pirineos Centrales, Formación y Subsecuente Inversión [Ph.D. thesis]: Barcelona, Spain, Universidad de Barcelona, 310 p.

Garrido, A., and Ríos, L., 1972, Síntesis geológica del Secundario y Terciario entre los ríos cinca y Segre (Pirineo Central de la vertiente surpirenaica, provincias de Huesca y Lérida): Boletín Geológico y Minero, v. 83, p. 1–47.

Grosfils, E.B., Schultz, R.A., and Kroeger, G., 2003, Geophysical exploration within northern Devils Lane graben, Canyonlands National Park, Utah: Implications for sediment thickness and tectonic evolution: Journal of Structural Geology, v. 25, p. 455–467, doi:10.1016/S0191-8141(02)00040-8.

Gutiérrez, F., 2004, Origin of the salt valleys in the Canyonlands section of the Colorado Plateau: Evaporite-dissolution collapse versus tectonic subsidence: Geomorphology, v. 57, p. 423–435.

Gutiérrez, F., and Cooper, A.H., 2012, Surface morphology of gypsum karst, *in* Frumkin, A., ed., Treatise on Geomorphology: Amsterdam, Elsevier (in press).

Gutiérrez, F., Ortuño, M., Lucha, P., Guerrero, J., Acosta, E., Coratza, P., Piacentini, D., and Soldati, M., 2008, Late Quaternary episodic displacement on a sackung scarp in the central Spanish Pyrenees: Secondary paleoseismic evidence?: Geodinamica Acta, v. 21, no. 4, p. 187–202, doi:10.3166/ga.21.187-202.

Gutiérrez, F., Galve, J.P., Lucha, P., Bonachea, J., Jordá, L., and Jordá, R., 2009, Investigation of a large collapse sinkhole affecting a multi-storey building by means of geophysics and the trenching technique, Zaragoza city, NE Spain: Environmental Geology, v. 58, p. 1107–1122, doi:10.1007/s00254-008-1590-8.

Gutiérrez, F., Lucha, P., and Galve, J.P., 2010, Reconstructing the geochronological evolution of large landslides by means of the trenching technique in the Yesa Reservoir Spanish Pyrenees: Geomorphology, v. 124, p. 124–136, doi:10.1016/j.geomorph.2010.04.015.

Gutiérrez, F., Guerrero, J., Galve, J.P., Lucha, P., García-Ruiz, J.M., Bonachea, J., and Carbonel, D., 2011, Detailed mapping of landslides in the Gállego glacial Valley (Spanish Pyrenees) as a basis for hazard analysis and risk mitigation, *in* Asrat, A., Dramis, F., Nyssen, J., and Umer, M., eds., Regional Conference of the International Association of Geomorphologists: Geomorphology for human adaptation to changing tropical environments: Addis Ababa, Ethiopia, p. 75.

Gutiérrez, F., Carbonel, D., Guerrero, J., McCalpin, J.P., Linares, R., Roque, C., and Zarroca, C., 2012, Late Holocene episodic displacement on fault scarps related to interstratal dissolution of evaporites (Teruel Neogene graben, NE Spain): Journal of Structural Geology, v. 34, p. 2–19, doi:10.1016/j.jsg.2011.11.006.

Harrison, J.V., 1927, Colorado-Utah salt domes: American Association of Petroleum Geologists Bulletin, v. 11, no. 2, p. 111–133.

Hartevelt, J.J.A., 1970, Geology of the upper Segre and Valira valleys, central Pyrenees, Andorra/Spain: Leidse Geologische Mededelingen, v. 45, p. 349–354.

Hudec, M.R., and Jackson, M.P.A., 2007, Terra infirma: Understanding salt tectonics: Earth-Science Reviews, v. 82, no. 1–2, p. 1–28, doi:10.1016/j.earscirev.2007.01.001.

Huntoon, P.W., 1982, The Meander anticline, Canyonlands, Utah: An unloading structure resulting from horizontal gliding on salt: Geological Society of America Bulletin, v. 93, p. 941–950, doi:10.1130/0016-7606(1982)93<941:TMACUA>2.0.CO;2.

Jackson, M.P.A., 1995, Retrospective salt tectonics, *in* Jackson, M.P.A., Roberts, D.G., and Snelson, S., eds., Salt Tectonics: A Global Perspective: American Association of Petroleum Geologists Memoir 65, p. 1–28.

Kirkham, R.M., Streufert, R.K., Kunk, M.J., Budahn, J.R., Hudson, M.R., and Perry, W.J., 2002, Evaporite tectonism in the lower Roaring Fork River valley, west-central Colorado, *in* Kirkham, R.M., Scott, R.B., and Judkins, T.W., eds., Late Cenozoic Evaporite Tectonism and Volcanism in West-Central Colorado: Geological Society of America Special Paper 366, p. 73–99.

Klimowitz, J., and Torrescusa, S., 1990, Notas sobre la estratigrafía y facies de la serie triásica en el Alóctono Surpirenaico, *in* Ortí, F., and Salvany, J.M., eds., Formaciones Evaporíticas de la Cuenca del Ebro y Cadenas Periféricas, y de la Zona de Levante: Barcelona, Spain, Empresa Nacional de Residuos Radiactivos Sociedad Anónima (ENRESA), p. 29–33.

Lanaja, J.M., Querol, R., and Navarro, A., 1987, Contribución de la Exploración Petrolífera al Conocimiento de la Geología de España: Madrid, Spain, Instituto Geológico y Minero de España (IGME), 465 p.

Linares, R., Rosell, J., Roqué, C., and Gutiérrez, F., 2010, Origin and evolution of tufa mounds related to artesian karstic springs in Isona area (Pyrenees, NE Spain): Geodinamica Acta, v. 23, no. 1–3, p. 129–150, doi:10.3166/ga.23.129-150.

Loke, M.H., 2011, Electrical imaging surveys for environmental and engineering studies—A practical guide to 2D and 3D surveys: Peneng, Malaysia, http://www.geoelectrical.com/coursenotes.zip (accessed 2011).

Loke, M.H., and Barker, R.D., 1996, Rapid least-squares inversion of apparent resistivity of pseudosections by a quasi-Newton method: Geophysical Prospecting, v. 44, p. 131–152, doi:10.1111/j.1365-2478.1996.tb00142.x.

Lucha, P., Gutiérrez, F., Galve, J.P., and Guerrero, J., 2012, Geomorphic and stratigraphic evidence of incision-induced halokinetic uplift and dissolution subsidence in transverse drainages crossing the evaporite-cored Barbastro-Balaguer anticline (Ebro Basin, NE Spain): Geomorphology (in press).

Marsic, S.D., Owen, S.E., and Crider, J.G., 2003, Distribution of displacement across Canyonlands Grabens using GPA and InSAR: Eos (Transactions, American Geophysical Union), Fall Meeting supplement, abstract G21D-0289.

Martínez, R., 1982, Ammonoideos Cretácicos del Prepirineo de la Provincia de Lleida [Ph.D. thesis]: Barcelona, Spain, Universidad Autónoma de Barcelona, 197 p.

Martinsen, O., 1994, Mass movements, *in* Maltman, A., ed., The Geological Deformation of Sediments: London, UK, Chapman & Hall, p. 127–165.

Mauduit, T., Guerin, G., Brun, J.-P., and Lecanu, H., 1997, Raft tectonics: The effects of basal slope angle and sedimentation rate on progressive extension: Journal of Structural Geology, v. 19, p. 1219–1230, doi:10.1016/S0191-8141(97)00037-0.

McCalpin, J.P., 1987, Recommended setback distances from active normal faults, *in* McCalpin, J.P., ed., Proceedings of the 23rd Symposium on Engineering Geology and Soils Engineering: Logan, Utah, p. 35–56.

McCalpin, J., 1999, Criteria for determining the seismic significance of sackungen and other scarplike landforms in mountainous regions, *in* Hanson, K.L., Kelson, K.I., Angell, M.A., and Lettis, W.R., eds.,Techniques for Identifying Faults and Determining their Origins: Washington, D.C., U.S. Nuclear Regulatory Commission, p. 2.55–2.59.

McCalpin, J.P., 2008, Reevaluation of geologic hazards in a mountain setting:The case of the Climax 7.5′ Quadrangle, Central Colorado, *in* 33rd International Geological Congress Abstracts: Oslo, Norway, http://www.cprm.gov.br/33IGC/1342266.html (accessed 26 April 2012).

McCalpin, J.P., 2009a, Field techniques in paleoseismology—Terrestrial environments, *in* McCalpin, J.P., ed., Paleoseismology: San Diego, Academic Press, p. 29–117.

McCalpin, J.P., 2009b, Paleoseismology in extensional tectonic environments, *in* McCalpin, J.P., ed., Paleoseismology: San Diego, Academic Press, p. 171–204.

McCalpin, J.P., 2009c, Application of paleoseismic data to seismic hazard assessment and neotectonic research, *in* McCalpin, J.P., ed., Paleoseismology: San Diego, Academic Press, available at: http://www.elsevierdirect.com/companions/9780123735768.

McCalpin, J.P., and Hart, E.W., 2003, Ridge-top spreading features and relationship to earthquakes, San Gabriel Mountains region, Southern California—Parts A and B, *in* Hart, E.W., ed., Ridge-Top Spreading in California; Contributions toward Understanding a Significant Seismic Hazard: Sacramento, California, California Geological Survey, CD 2003-05, 2 CD-ROMs.

McCalpin, J.P., Bruhn, R.L., Pavlis, T.L., Gutierrez, F., Guerrero, J., and Lucha, P., 2011, Antislope scarps, gravitational spreading, and tectonic faulting in the western Yakutat microplate, south coastal Alaska: Geosphere, v. 7, p. 1143–1158, doi:10.1130/GES00594.1.

McCleary, J., Dohrenwend, J., Cluff, L., and Hanson, K., 1978, 1872 Earthquake Studies: Washington Public Power Supply System Nuclear Project 1 and 4: San Francisco, California, report by Woodward-Clyde Consultants, submitted to United Engineers and Constructors, Inc., April 1978, contract no. 52028, 75 p. (plus appendices).

McGill, G.E., and Stromquist, A.W., 1979, The grabens of Canyonlands National Park, Utah: Geometry, mechanics and kinematics: Journal of Geophysical Research, v. 84, p. 4547–4563, doi:10.1029/JB084iB09p04547.

Mège, D., Le Deit, L., Rango, T., Jourdan, F., Tesfaye, K., López-González, T., and Purcell, P., 2011, Large-scale gravitational spreading in southeast Ethiopia, *in* Asrat, A., Dramis, F., Nyssen, J., and Umer, M., eds., Geomorphology for Human Adaptation to Changing Tropical Environments: Addis Ababa, Ethiopia, p. 96.

Mellere, D., and Marzo, M., 1992, Los depósitos aluviales sintectónicos de la Pobla de Segur: Alogrupos y su significado tectonoestratigráfico: Acta Geológica Hispánica, v. 27, p. 145–159.

Mey, P.H.W., Nagtegaal, P.J.C., Roberti, K.J., and Hartevelt, J.J.A., 1968, Lithostratigraphic subdivision of post-Hercynian deposits in the south-central Pyrenees, Spain: Leidse Geologische Mededelingen, v. 41, p. 221–228.

Micallef, A., Masson, D.G., Berndt, Ch., and Stow, D.A.V., 2007, Morphology and mechanics of submarine spreading: A case study from the Storegga Slide: Journal of Geophysical Research, v. 112, F03023, doi:10.1029/2006JF000739.

Moore, J.M., and Schultz, R.A., 1999, Processes of faulting in jointed rocks in Canyonlands National Park, Utah: Geological Society of America Bulletin, v. 111, p. 808–822, doi:10.1130/0016-7606(1999)111<0808:POFIJR>2.3.CO;2.

Muñoz, J.A., 1988, Estructura de las unidades surpirenaicas en la transversal del corte ECORS, *in* Field Gide Reunión Extraordinaria ECORSPIRINEOS: Baussens-Balaguer, Spain, Sociedad Geológica de España and Société Géologique de France.

Muñoz, J.A., 1992, Evolution of a continental collision belt: ECORS-Pyrenees crustal balanced cross-section, *in* McClay, K.R., ed., Thrust Tectonics: London, Chapman and Hall, p. 235–246.

Nicolas, M., Santoire, J.P., and Delpech, P.Y., 1990, Intraplate seismicity: New seismotectonic data in Western Europe: Tectonophysics, v. 179, p. 27–53, doi:10.1016/0040-1951(90)90354-B.

Olivera, C., Redondo, E., Lambert, J., Riera Melis, A., and Roca, A., 2006, Els Terratrèmols dels Segles XIV i XV a Catalunya: Institut Cartogràfic de Catalunya Monografies 30, 407 p.

Ortuño, M., Queralt, P., Martí, A., Ledo, J., Masana, E., Perea, H., and Santanach, P., 2008, The North Maladeta fault (Spanish central Pyrenees) as the Vielha 1923 earthquake seismic source: Recent activity revealed by geomorphological and geophysical research: Tectonophysics, v. 453, p. 246–262, doi:10.1016/j.tecto.2007.06.016.

Pánek, T., Hradecký, J., Smolková, V., and Šilhán, K., 2008, Giant ancient landslide in the Alma water gap (Crimean Mountains, Ukraine): Notes to the predisposition, structure, and chronology: Landslides, v. 5, p. 367–378, doi:10.1007/s10346-008-0129-0.

Pánek, T., Tábořík, P., Klimeš, J., Komárková, V., Hradecký, J., and Šťastnýc, M., 2011, Deep-seated gravitational slope deformations in the highest parts of the Czech Flysch Carpathians: Evolutionary model based on kinematic analysis, electrical imaging and trenching:

Geomorphology, v. 129, no. 1–2, p. 92–112, doi:10.1016/j.geomorph.2011.01.016.

Pasuto, A., and Soldati, M., 1996, Rock spreading, *in* Dikau, R., Brunsden, D., Schrott, L., and Ibsen, M.-L., eds., Landslide Recognition: Identification, Movement and Causes: Chichester, UK, John Wiley & Sons, p. 122–136.

Petro, L., Vlcko, J., Ondrasik, R., and Polascinova, E., 2004, Recent tectonics and slope failures in the Western Carpathians: Engineering Geology, v. 74, p. 103–112, doi:10.1016/j.enggeo.2004.03.004.

Peybernés, 1976, Le Jurassique et le Crétacé Inférieur des Pyrénées Franco-Espagnoles entre la Garonne et la Méditerranée [Ph.D. thesis]: Toulouse, France, Service de Reprographie, Académie de Toulouse, 459 p.

Potter, D.B., and McGill, G., 1978, Valley anticlines of the Needles District, Canyonlands National Park, Utah: Geological Society of America Bulletin, v. 89, no. 6, p. 952–960, doi:10.1130/0016-7606(1978)89<952:VAOTND>2.0.CO;2.

Radbruch-Hall, D., 1978, Gravitational creep of rock masses on slopes, *in* Voight, B., ed., Rockslides and Avalanches—Natural Phenomena: Developments in Geotechnical Engineering, Volume 14A: Amsterdam, Netherlands, Elsevier, p. 608–657.

Reimer, P.J., Baillie, M.G.L., Bard, E., Bayliss, A., Beck, J.W., Bertrand, C., Blackwell, P.G., Buck, C.E., Burr, G., Cutler, K.B., Damon, P.E., Edwards, R.L., Fairbanks, R.G., Friedrich, M., Guilderson, T.P., Hughen, K.A., Kromer, B., McCormac, F.G., Manning, S., Bronk Ramsey, C., Reimer, R.W., Remmele, S., Southon, J.R., Stuiver, M., Talamo, S., Taylor, F.W., van der Plicht, J., and Weyhenmeyer, C.E., 2009, IntCal09 and Marine09 radiocarbon age calibration curves, 0–50,000 years cal BP: Radiocarbon, v. 51, p. 1111–1150.

Rohn, J., Resch, M., Schneider, H., Fernandez-Steeger, T.M., and Czurda, K., 2004, Large-scale lateral spreading and related mass movements in the Northern Calcareous Alps: Bulletin of Engineering Geology and the Environment, v. 63, p. 71–75, doi:10.1007/s10064-003-0201-x.

Rosell, J., 1963, Estudio Geológico del Sector del Prepirineo Comprendido entre los Ríos Segre y Noguera Ribagorzana (Prov. de Lérida) [Ph.D. thesis]: Barcelona, Spain, Universidad de Barcelona, 225 p.

Rosell, J., 1970, Mapa Geológico de España, Hoja no. 252—Tremp: Madrid, Spain, Instituto Geológico y Minero de España, scale 1:50,000, Primera Serie.

Rosell, J., 1994, Mapa Geológico de España Hoja no. 252—Tremp: Madrid, Spain, Instituto Geológico y Minero de España, scale 1:50,000, Segunda Serie.

Rosell, J., and Linares, R., 2001, Grandes deslizamientos en el frente de la lámina cabalgante del Montsec (Sierra del Montsec, Prepirineo Central): Revista de la Sociedad Geológica de España, v. 14, no. 3–4, p. 255–268.

Rosell, J., and Llompart, C., 1982, Pirineo, *in* El Cretácico de España: Madrid, Spain, Universidad Complutense, Universidad Complutense de Madrid, p. 161–198.

Rosell, J., and Riba, O., 1966, Nota sobre la disposición sedimentaria de los conglomerados de la Pobla de Segur (Província de Lérida), *in* Actas V Congreso Estudios Pirenaicos: Jaca-Pamplona, Instituto de Estudios Pirenaicos, 16 p.

Rowan, M.G., Jackson, M.P.A., and Trudgill, B.D., 1999, Salt-related fault families and fault welds in the northern Gulf of Mexico: American Association of Petroleum Geologists Bulletin, v. 83, p. 1454–1484.

Salvany, J.M., and Bastida, J., 2004, Análisis litoestratigráfico del Keuper surpirenaico central: Revista de la Sociedad Geológica de España, v. 17, no. 1–2, p. 3–26.

Saura, E., 2004, Anàlisi Estructural de la Zona de les Nogueres, Pirineus Centrals [Ph.D. thesis]: Barcelona, Spain, Universitat Autònoma de Barcelona, 355 p.

Saura, E., and Teixell, A., 2000, Relación entre los conglomerados oligocenos y las estructuras tectónicas en la zona de Les Nogueres, Pirineo Central: Geotemas, v. 1, no. 2, p. 201–203.

Schlische, R.W., Young, S.S., Ackermann, R.V., and Gupta, A., 1996, Geometry and scaling relations of a population of very small rift-related normal faults: Geology, v. 24, p. 683–686, doi:10.1130/0091-7613(1996)024<0683:GASROA>2.3.CO;2.

Schrott, L., and Sass, O., 2008, Application of field geophysics in geomorphology: Advances and limitations exemplified by case studies: Geomorphology, v. 93, p. 55–73, doi:10.1016/j.geomorph.2006.12.024.

Schultz-Ela, D.D., 2001, Excursus on gravity gliding and gravity spreading: Journal of Structural Geology, v. 23, p. 725–731, doi:10.1016/S0191-8141(01)00004-9.

Seguret, M., 1972, Etude Tectonique des Nappes et Séries Décollés de la Partie Centrale du Versant Sud des Pyrenées: Caractère Synsédimentaire, Rôle de la Compression et de la Gravité [Ph.D. thesis]: Montpellier, France, Université de Montpellier, Publications de l'Université des Sciences et Techniques du Languedoc (USTELA), Série Géologie Structurale, v. 2, 210 p.

Simpson, G., 2004, Role of river incision in enhancing deformation: Geology, v. 32, no. 4, p. 341–344, doi:10.1130/G20190.2.

Susagna, T., Roca, A., Goula, X., and Batlló, J., 1994, Analysis of macroseismic and instrumental data for the study of the 19 November 1923 earthquake in the Aran Valley (central Pyrenees): Natural Hazards, v. 10, p. 7–17, doi:10.1007/BF00643438.

Tran, M.K., Shin, H., Byun, Y.-H., and Lee, J.-S., 2011, Mineral dissolution effects on mechanical strength: Engineering Geology, v. 125, p. 26–34, doi:10.1016/j.enggeo.2011.10.014.

Trudgill, B.D., 2002, Structural controls on drainage development in the Canyonlands grabens of southeast Utah: American Association of Petroleum Geologists Bulletin, v. 86, p. 1095–1112.

Trudgill, B.D., and Cartwright, J.A., 1994, Relay ramp forms and normal fault linkages, Canyonlands National Park, Utah: Geological Society of America Bulletin, v. 106, p. 1143–1157, doi:10.1130/0016-7606(1994)106<1143:RRFANF>2.3.CO;2.

Van Dam, R.L., 2010, Landform characterization using geophysics—Recent advances, applications, and emerging tools: Geomorphology, v. 137, p. 57–73, doi:10.1016/j.geomorph.2010.09.005.

Varnes, D.J., 1978, Slope movement types and processes, *in* Schuster, R.L., and Krizek, R.J., eds., Landslides: Analysis and Control: Washington, D.C., National Academy of Sciences, p. 11–33.

Viero, A., Teza, G., Massironi, M., Jaboyedoff, M., and Galgaro, A., 2010, Laser scanning-based recognition of rotation movements on a deep seated gravitational stability: The Cinque Torri case (north-eastern Italian Alps): Geomorphology, v. 122, p. 191–204, doi:10.1016/j.geomorph.2010.06.014.

Vlcko, J., 2004, Extremely slow slope movements influencing the stability of Spis Castle, UNESCO site: Landslides, v. 1, p. 67–71, doi:10.1007/s10346-003-0007-8.

Warren, J.K., 2006, Evaporites. Sediments, Resources and Hydrocarbons: Heidelberg, Germany, Springer, 1035 p.

Zarroca, M., Linares, R., Bach, J., Roqué, C., Moreno, V., Font, Ll., and Baixeras, C., 2012, Integrated geophysics and soil gas profiles as a tool to characterize active faults: The Amer fault example (Pyrenees, NE Spain): Environmental Earth Sciences, doi:10.1007/s12665-012-1537-y.

Záruba, Q., and Mencl, V., 1982, Landslides and their Control: Amsterdam, Netherlands, Elsevier, 324 p.

MANUSCRIPT RECEIVED 27 JANUARY 2012
REVISED MANUSCRIPT RECEIVED 12 APRIL 2012
MANUSCRIPT ACCEPTED 12 APRIL 2012
Printed in the USA